Journal of Molecular Structure 1325 (2025) 141285

Contents lists available at ScienceDirect

Journal of Molecular Structure

journal homepage: www.elsevier.com/locate/molstr

A new Ag(I)-complex of 5-chloroquinolin-8-ol ligand: Synthesis, spectroscopic characterization, and DFT investigations, in vitro antioxidant (DPPH and ABTS), α-glucosidase, α-amylase inhibitory activities with protein-binding analysis

Ceyhun Kucuk [a,*], Sibel Celik [b], Senay Yurdakul [c], Ebru Coteli [b]

[a] Ahmet Erdogan Vocational School of Health Services, Zonguldak Bulent Ecevit University, Zonguldak, Turkey
[b] Vocational School of Health Services, Kırsehir Ahi Evran University, Kırşehir 40100, Turkey
[c] Department of Physics, Faculty of Science, Gazi University, Ankara, Turkey

ARTICLE INFO

Keywords:
5-Chloroquinolin-8-ol
DFT
QTAIM
Antidiabetic
Antioxidant
Molecular docking

ABSTRACT

We report the synthesis and characterization of a new silver complex of 5-chloroquinolin-8-ol ([Ag($C_9H_5ClNO)_2NO_3$]). The Ag(I) complex was characterized using elemental analysis and various spectral techniques such as Fourier-transform infrared (FT-IR), ^{1}H nuclear magnetic resonance (NMR), and ultraviolet–visible (UV-Vis) spectra. Structural features and intramolecular interactions have been investigated with quantum mechanical calculations using density functional theory (DFT) calculations. Frontier molecular orbital energies revealed an energy band gap of 1.08 eV, indicating that there is charge transfer within the molecule. In experimentally recorded UV-Vis spectra, electronic transitions demonstrated the ability to conduct charges. We conducted topological analyses such as electron localization function (ELF), localized orbital locator (LOL), quantum theory of atoms in molecules (QTAIM), and reduced density gradient (RDG) to identify the van der Waals interaction and steric effect, and also forecasted global reactivity parameters and Fukui functions. Natural bond orbital (NBO) analysis detects charge transfer, hydrogen bonding, and hyperconjugative interactions that stabilize the structure. This work assessed the title complex's in vitro antioxidant and antidiabetic properties. The scavenging effect of the complex on both radicals was observed. In particular, it was determined that the DPPH$^\bullet$ radical-scavenging effect was greater than the ABTS$^{\bullet+}$ radical. Additionally, in the determination of antidiabetic activity, α-glucosidase enzyme activity was found to be higher than α-amylase enzyme activity. The in vitro potential was validated utilizing molecular docking investigations against target receptors.

1. Introduction

The 8-hydroxyquinoline skeleton is an intriguing structure for the design and synthesis of novel biologically active heterocyclic compounds [1]. The 8-hydroxyquinoline (8-HQ) is a tiny planer molecule that can chelate metals and has a lipophilic effect. Consequently, 8-HQ and its derivatives have anti-inflammatory, anti-cancer, antioxidant, anti-neurodegenerative, and antidiabetic effects [2]. Also, the 8-HQ-based organic compounds are more biologically active molecules with several electrophilic and nucleophilic reactive regions [3]. These compounds have grown increasingly relevant in recent years due to their potential qualities in a variety of sectors, including anticorrosion and complexing properties of metals [1]. Quinoline derivatives are also used as chelating agents due to their N-donor ligands to form complex compounds with metallic ions in coordination chemistry and are of great interest for the possibility of enhancing biological activities [4,5]. Metal ions, which are a component of coordination complexes for many biological reactions, either promote or suppress biological reactions [6]. Several investigations have shown that natural/synthetic quinoline-based metal complexes have enormous promise as anticancer and antidiabetic medicines, with minimal side effects and maximum function [7,8]. Transition metals such as silver, cobalt, and copper play an important role in the development of new metal-based medications to treat a wide range of human and animal diseases [9]. Recently, scientists have been investigating the anti-diabetic properties of hydroxyquinolinone [8,10]. Recent advances in medicinal chemistry play a

* Corresponding author.
E-mail address: ceyhun.kucuk@beun.edu.tr (C. Kucuk).

https://doi.org/10.1016/j.molstruc.2024.141285
Received 11 November 2024; Received in revised form 25 December 2024; Accepted 30 December 2024
Available online 1 January 2025

significant role in the diabetes mellitus treatment of metal complexes. In designing new therapeutic drugs, complexes of transition metal have been observed to be forceful in the treatment of this chronic disorder that cannot be countered by pure organic compounds [11]. Moreover, mixed ligand complexes derived from 8-HQ used as antioxidants have a noticeable effect on reducing mortality in brine shrimp, and mixed ligand complexes play an important role in the science of luminescence because they are highly colorful and stable [12]. Due to these properties, it has become important to examine the complexes of 8-HQ-derived ligands. Kale et al. [2] synthesized the metal (II), (IV), and (VI) coordination compounds of 8-Hydroxyquinoline, Ni2+, Cu2+, Co2+, and Mn2+ and characterized them using UV-Visible and ADME, thus determining the drug similarity, physicochemicals and pharmacokinetics. Also, Rodr Mguez-Franco and co-workers [13] reported that some 8-HQ-related complexes showed neuroprotective activity, which was associated with their ability to complex redox-active metals and reduce neurotoxicity, thus becoming novel multitarget-directed ligands (MTDLs) for the treatment of Alzheimer's disease [13].

In the current study, the Ag(I) complex of the bioactive ligand 5-chloroquinolin-8-ol (5Cl8HQ) was synthesized and fully characterized using standard spectroscopic methods such as ^{1}H NMR, FT-IR, UV-Vis, and elemental analysis. The synthesized compounds were subjected to quantum chemical calculations at DFT to shed light on their electronic and chemical reactivity properties. The DFT studies are appropriately used to accelerate large-scale drug evaluation [14] as they provide information on structural stability, reactivity, and spectroscopic properties, as well as biological interactions and activities. A literature search reveals that a combination of experimental and computational approaches for molecular structure, spectroscopy, and docking studies of organic molecules is currently frequently used [15]. Therapeutic approaches to combat oxidative stress-related diseases are crucial for reducing the prevalence of diabetes worldwide and improving the lives of those affected, so focus has been placed on the antioxidant and antidiabetic activities of the title silver complex. In order to find the possible molecular interaction between the α-amylase and α-glucosidase enzymes and the compound, we also performed molecular docking analysis to determine the efficacy of the compound for the treatment of diabetes. The calculated binding energy values of the receptors with Ag (I) complex were compared to in vitro studies.

2. Materials and methods

2.1. Computational methods

The DFT calculations were performed using the Gaussian 09 software package [16], and the visuals for these computations were generated using the Gauss View 5.0.9 software [17]. The $[Ag(C_9H_5ClNO)_2NO_3]$ complex was optimized using the Becke-3-Lee-Yang-Parr (B3LYP) functional [18,19] and the Stuttgart Dresden triple zeta ECPs Effective-Core Potential (SDD) basis set [20,21]. Additionally, frequency and electronic property calculations for the optimized structure were performed using the same functional and basis set in the DFT method. UV-Vis calculation for the synthesized complex was performed by applying the TD-DFT/CAM-B3LYP/SDD level of theory [22,23] using the IEFPCM model [24] in ethanol solvent. The calculation for the free ligand was carried out using the 6-311++G(d,p) basis set [25]. The Multiwfn software package program was used to generate ELF and LOL surface maps, dual descriptor images, RDG, and non-covalent interaction (NCI) analysis [26,27]. Given the high computational costs, the direct application of DFT to complex biomolecular systems is limited and restrictive in terms of the treatable size of the given systems. To overcome these limitations, the Autodock program was used for larger systems that encapsulate a larger portion of protein molecules. Autodock 2.2.6 was used to carry out the molecular docking of the chemical ligand-protein binding site. RCSB is the main source of protein data bank (PDB) structures that are used as target proteins. With Discover Studio Visualizer, the nonbonding interactions of the receptor pocket's active site are investigated [28,29].

2.2. Experimental methods

2.2.1. Synthesis

5Cl8HQ (95% purity), silver nitate (99.5% purity), and ethanol (99.8%) were obtained from Sigma Aldrich Chemical Company. During the synthesis phase, solutions were prepared in ethanol for both molecules without an additional purification process. In the first stage, we prepared a 2 mmol 5Cl8HQ solution in 20 ml of ethanol and mixed it with a magnetic stirrer for 10 min at 50°C. In the second stage, 1 mmol $AgNO_3$ solution in 20 ml of ethanol was prepared and mixed for 5 min at 50°C. In the final stage, we added the prepared AgNO3 solution dropwise to the 5Cl8HQ solution, stirred at 50°C for 60 min, and obtained a white precipitate. We conducted an elemental analysis to ascertain the chemical formula of the resulting complex. In the resulting complex, the experimental and theoretical percentage ratios for C, H, and N atoms are as follows: $[Ag(C_9H_5ClNO)_2NO_3]$ CHN Exp: C: 41.47%, H: 2.01%, N: 7.43%, and Calc: C: 41.01%, H: 1.91%, N: 7.97%. The synthesized complex has 79% efficiency.

2.2.2. Antioxidant activity

2.2.2.1. In vitro determination of DPPH• radical scavenging activity. The most commonly used spectrophotometric method to measure antioxidant activity is the DPPH• radical scavenging method [30]. The antioxidant capacity of $[Ag(C_9H_5ClNO)_2NO_3]$ was evaluated using the radical DPPH• (2,2-diphenyl-1-picrylhydrazyl). For this purpose, 0.5 ml was taken from the samples prepared at 25, 50, and 100 μg/mL concentrations. Then, 2 mL of DPPH• radical solution prepared at a 0.1 mM concentration was added. The samples were kept in a dark environment for 30 min. Then, the absorbance of the samples was determined at 517 nm. The standard materials are ascorbic acid and butylated hydroxytoluene (BHT). The results were calculated using the formula below.

$$\%\text{Inhibition} = \frac{[(AC - AS)]}{AC} \times 100 \quad (1)$$

AC: *Absorbance control*
AS: *Absorbance sample*

The samples' IC_{50} (inhibitor concentration) and inhibition percentages were computed. The results were compared with the standard substance.

2.2.2.2. In vitro ABTS•+ radical scavenging activity. The antioxidant activity of the complex was determined using the ABTS•+ [2,2′-Azino-bis (3-ethylbenzthiazoline-6-sulfonic acid)] cationic radical [31]. 7 mM ABTS solution prepared using pure water and 2.45 mM $Na_2S_2O_8$ solution were mixed at a ratio of 1:05. This mixture was mixed in the dark environment for 16 h. In this way, radical formation was achieved. The prepared radical solution was tightly wrapped with aluminum foil. The absorbance of the radical solution was prepared to be 0.7 by using an 80% ethanol-water mixture. This radical solution was used in the experiments. Samples were prepared from (complex, standard ascorbic acid, and BHT) at concentrations of 25, 50, and 100 μg/mL. 50 μl of each sample was taken. Then 2 mL of radical solution was added. Complex and standard samples were stored in a dark setting for 30 min under room temperature. The absorbance of all samples was determined at 734 nm. The inhibition values of the samples were determined using the formula below.

$$\%\text{Inhibition} = \frac{[(AC - AS)]}{AC} \times 100 \quad (2)$$

AC: *Absorbance control*
AS: *Absorbance sample*

Again, all samples' IC_{50} values were calculated and compared to

standard values.

2.2.3. Antidiabetic activity

2.2.3.1. In vitro α-amylase enzyme inhibition. α-Amylase enzyme activity was determined in the presence and absence of $[Ag(C_9H_5ClNO)_2NO_3]$ [32]. For this purpose, 0.5 mL of starch and 0.5 mL of enzyme solution were mixed and left at room temperature for 20 min. One milliliter of DNS (3,5-dinitrosalicylic acid) solution was added and heated for five minutes. The samples were chilled before being diluted with 7.5 mL of distilled water. At 540 nm, the samples' absorbance was measured. Samples were generated at doses of 25, 50, and 100 μg/mL to examine if the extracts had an inhibiting impact on the α-amylase enzyme. Then, the same amount (0.5 mL) of sample and enzyme was mixed and kept at 37°C for 15 min. Starch (0.5 mL) was added. Following the addition of 1 mL of DNS (3,5-dinitrosalicylic acid), the samples were heated to a boil. A sample blank was run for each sample. The same procedures were applied to standard acarbose. The α-amylase enzyme inhibition values of the samples or acarbose were calculated using the formula below.

$$\%\text{Inhibition} = \frac{[(AA - AE)]}{AA} \times 100 \quad (3)$$

AA *= Absorbance Amylase (the absorbance of the tube is considered 100% active)*

AE*= Absorbance Extract (sample absorbance-sample blank absorbance)*

2.2.3.2. α-Glucosidase enzyme inhibition. α−Glucosidase is used in the treatment of non-insulin-dependent diabetes. Inhibitors have an important place in the antidiabetic drug industry [33]. In determining α-glucosidase enzyme activity, it was measured both in the presence and absence of the complex [34]. First, the amount of substrate to be added to the medium was determined. For this purpose, saturation substrate concentration was investigated by studying enzyme activity in different amounts (20, 40, 60, 80, 100, and 120 μL) of a 5 mM p-NPG solution. This concentration was determined to be 100 μL and added to the reaction medium. Enzyme solutions (20 μL) and 100 μL p-NPG were combined, and the mixture was incubated for 15 min at 37°C to determine the enzyme activity. 80 μL of a 0.1 M Na_2CO_3 solution was added to the samples. Absorbance measurements were made at 405 nm. To determine whether the $[Ag(C_9H_5ClNO)_2NO_3]$ complex has an inhibitory effect on the α-glucosidase enzyme, solutions were prepared at concentrations of 1, 5, 7, and 10 mg/mL. 50 μL of these solutions was taken and incubated with 20 μL of enzyme at 37°C for 10 min. 100 μL of substrate was added to the samples and left at 37°C for 20 min. 80 μL Na_2CO_3 was added, and absorbance measurements were made at λ = 405 nm. Acarbose, an enzyme inhibitor, was used as a positive control. The α-glucosidase enzyme inhibition percentages in each sample were determined using the formula below.

$$\%\text{Inhibition} = \frac{[(AG - AE)]}{AG} \times 100 \quad (4)$$

AG*= Absorbance Glucosidase (the absorbance of the tube is considered 100% active)*

AE*= Absorbance Extract (sample absorbance-sample blank absorbance)*

2.2.4. Statistical analysis

Three parallel measurements were made in all experiments. Results are presented as the arithmetic mean ± standard deviation. IC_{50} values were computed in addition to the samples' inhibition percentages. The results were expressed in tables and figures.

3. Results and discussion

3.1. Geometric parameters

The synthesized $[Ag(C_9H_5ClNO)_2NO_3]$ complex was optimized to determine its geometric parameters (bond lengths and bond angles) in the minimum energy state. A single crystal structure of the title complex could not be obtained. Therefore, to compare the geometric parameters, XRD data of different complexes that are structurally similar, as well as the main ligand used in the study, were used. Geometric parameters were listed in supplementary Table S1, and the optimized geometric parameters were presented in Fig. 1.

The Ag atom is coordinated in the N and O atoms of the two 5Cl8HQ molecules in the synthesized structure. For the optimized structure, the O_1-Ag_{34} and O_2-Ag_{34} bond lengths were calculated as 2.029 Å, and the N_3-Ag_{34} and N_4-Ag_{34} bond lengths were calculated as 2.061 and 2.088 Å, respectively. For the bis(8-hydroxyquinoline)silver(I) [35] and aqua (8-hydroxyquinoline-5-sulfonato-k^2N,O^8)silver(I) monohydrate [36] complexes, the O_1-Ag_{34} and O2-Ag_{34} bond lengths were reported as 2.505 and 2.446 Å, while N_3-Ag_{34} and N_4-Ag_{34} bond lengths were reported as 2.145 and 2.196 Å. N_3-C_5/N_4-C_{20} and N_3-C_{16}/N_4-C_{30} bond lengths were calculated as 1.383 and 1.332 Å. In the crystal data of the 5-chloro-8-hydroxyquinoline molecule, the values corresponding to the N_3-C_5 and N_3-C_{16} bond lengths are 1.368 and 1.322 Å [37]. While the C_{11}-Cl_{19} and C_{26}-Cl_{39} bond lengths of the title complex were found to be 1.823 Å in theoretical calculations, this value was reported as 1.741 Å for the crystal data of the 5-chloro-8-hydroxyquinoline molecule [37]. The bond lengths of Ag_{34}-O_{35} and Ag_{34}-O_{36} between the silver atom and the oxygen atoms of the nitrate group were calculated as 3.108 and 2.457 Å, respectively. The O_{35}-N_{38}, O_{36}-N_{38}, and O_{37}-N_{38} bond lengths between the oxygen atoms and the N atom of the nitrate group were calculated as 1.309, 1.337, and 1.277 Å.

The C_6-O_1-Ag_{34} and C_{21}-O_2-Ag_{34} bond angles of the synthesized complex were calculated as 110.79 and 111.21°, respectively. In the XRD data of bis(8-hydroxyquinoline)silver(I) [35] and aqua(8-hydroxyquinoline-5-sulfonato-k^2N,O^8)silver(I) monohydrate complexes [36], C_6-O_1-Ag_{34} angles were reported as 108.9 and 114.20°. While C_5-N_3-Ag_{34} and C_{20}-N_4-Ag_{34} bond angles were calculated as 110.55 and 110.08°, C_{16}-N_3-Ag_{34} and C30-N4-Ag34 angles were calculated as 127.12 and 127.61°. The C_5-N_3-Ag_{34} and C_{16}-N_3-Ag_{34} bond angle values of the samples whose XRD data are given supplementary Table S1 are reported as 119.7/120.42 [35] and 123.3/122.24° [36]. While the N_3-Ag_{34}-N_4 bond angle was calculated as 172.79° for the title complex, this value was given as 167.9 for the bis(8-hydroxyquinoline)silver(I) complex [35]. The O_1-Ag_{34}-O_2 bond angle calculated for the title complex was found to be 170.32°. For the bis(8-hydroxyquinoline)silver(I) complex, this value was reported as 109.9 [35]. Additionally, O_1-Ag_{34}-N_3, O_1-Ag_{34}-N_4, and O_2-Ag_{34}-N_3 bond angles were calculated as 82.58, 97.47, and 96.52°, respectively. The values corresponding to these angles in the bis(8-hydroxyquinoline)silver(I) complex are 71.7, 113.6, and 117.2° [35].

Root mean square deviation (RMSD) values were calculated to show the agreement between the XRD data used to compare the calculated bond lengths and bond angles for the synthesized complex in supplementary Table S1 [38]. In the comparison with the 5-chloro-8-hydroxyquinoline molecule, RMSD values for bond length and bond angles were

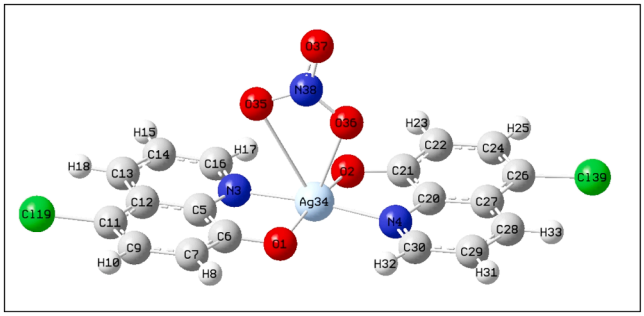

Fig. 1. Optimized geometric structure of the $[Ag(C_9H_5ClNO)_2NO_3]$ complex.

found to be 0.030 and 2.224, respectively. According to these results, the bond lengths and bond angles in the rings of the 5Cl8HQ molecule in the structure of the complex are quite compatible with the XRD data. In comparison with the bis(8-hydroxyquinoline)silver(I) complex, the RMSD value was calculated as 0.132 for bond length and 13.78 for bond angles. In comparison with the bis(8-hydroxyquinoline)silver(I) complex, the RMSD value was calculated as 0.132 for bond length and 13.78 for bond angles. The values obtained for bond lengths show that they are quite compatible with each other. But the bond angles are not very compatible. Additionally, the RMSD values calculated for the aqua (8-hydroxyquinoline-5-sulfonato-k^2N,O^8)silver(I) monohydrate complex were calculated as 0.12 for bond length and 4.46 for bond angle. These results show that there is harmony between bond lengths, while there are not very significant deviations in bond angles. The reason for the deviation observed between theoretical calculations and XRD data, especially for bond angles, can be explained as follows: Theoretical calculations are performed on a single molecule in the gas phase. However, in the crystal lattice, the molecule atoms are in coulombic interaction. Therefore, differences may be observed [39].

3.2. ^1H NMR analysis

The experimental ^1H NMR chemical shift values of the C_9H_6ClNO (5Cl8HQ) molecule and the synthesized $[Ag(C_9H_5ClNO)_2NO_3]$ complex from it are listed in Table 1, and the ^1H NMR spectra recorded in DMSO solvent are shown in Fig. 2. The signal observed at 10.24 ppm is assigned to the OH group attached to the benzene ring of the 5Cl8HQ ligand. The signal for the OH group of the 5CL8HQ ligand observed at 10.24 ppm was completely lost in the spectrum of the $[Ag(C_9H_5ClNO)_2NO_3]$ complex when the experimental spectra were looked at. This result provides clear evidence that the silver (Ag) atom bonds with the oxygen (O) atom of the -OH group in the quinoline ring. Looking at the literature, in one study, 8-Hydroxyquinoline derivative (1-(8-Hydroxy quinolin-2yl-methyl) thiourea ligand) and its metal (Zn(II), Cu(II), Ni(II), and Co (II)) complexes have been studied. In this study, the chemical shift value for the H atom belonging to the -OH group of 8-hydroxyquinoline was observed at 8.6 ppm, while the signal assigned to this group in the free ligand for the synthesized metal complexes completely disappeared, as in our study [40]. In another study, the complexation of 8-hydroxyquinoline-5-sulfonate with vanadium (V) was examined. In this study, structures with an almost octahedral geometry in a ratio of 1:2 (metal: ligand) were synthesized, with the central metal coordinated to two ligands. No shift was observed in the ^1H NMR spectra in the -OH group of these synthesized structures, and chemical shift values were assigned only for aromatic protons. That is, in this study, the metal atom bonded with the oxygen atom of the -OH group [41].

Aromatic protons of the free ligand are assigned at 8.96 (H_{17}), 8.51 (H_{18}), 7.74 (H_{15}), 7.63 (H_{10}), and 7.10 (H_8) ppm. No significant chemical shift was observed in the aromatic protons of the benzene and pyridine rings of the synthesized metal complex. The chemical shift values for $[Ag(C_9H_5ClNO)_2NO_3]$ are 8.98 (H_{17}/H_{32}), 8.55 (H_{18}/H_{33}), 7.78 (H_{15}/H_{31}), 7.64 (H_{10}/H_{25}), and 7.14 (H_8/H_{23}) ppm. While the signal assignments for aromatic protons for the 1-(8-hydroxy quinolin-2yl-methyl)thiourea ligand were reported in the range of 7.1–7.6 ppm, this range was stated as 7.1–7.4 for all synthesized metal complexes. No significant chemical shift values were observed for the aromatic protons of the metal complexes synthesized in this study [40]. Finally, signals for chemical shift values for aromatic protons are recorded in the range of approximately 7–8 ppm [42]. It can be said that the signal values obtained for the synthesized $[Ag(C_9H_5ClNO)_2NO_3]$ complex are also quite compatible with this observation range.

Table 1
Experimental ^1H NMR chemical shift values of 5Cl8HQ molecule and the $[Ag(C_9H_5ClNO)_2NO_3]$ complex.

C_9H_6ClNO (5Cl8HQ)		$[Ag(C_9H_5ClNO)_2NO_3]$	
Atom	ppm	Atom	Ppm
O-H	10.24	O-H	-
H_{17}	8.96	H_{17}/H_{32}	8.98
H_{18}	8.51	H_{18}/H_{33}	8.55
H_{15}	7.74	H_{15}/H_{31}	7.78
H_{10}	7.63	H_{10}/H_{25}	7.64
H_8	7.10	H_8/H_{23}	7.14

3.3. Vibrational analysis

Frequency values for the optimized geometric structure of the $[Ag(C_9H_5ClNO)_2NO_3]$ complex are calculated at the DFT/B3LYP/SDD level of theory [20]. The recorded Far-IR and FT-IR spectra of the free ligand and its synthesized Ag(I) complex are presented in Fig. 3. The IR spectrum obtained from theoretical calculations is presented in supplementary Fig. S1. Experimental and calculated frequency values of the synthesized complex are also listed in Table 2. Additionally, the recorded frequency values of the free ligand are found in this table to compare and explain the complexation. Mode assignments were performed according to the total energy distribution using the VEDA program, and those with a value of 10% or more are given.

When the experimental FT-IR spectrum of the synthesized Ag(I) complex is compared with that of the free ligand, the new peaks seen at 1361 (vs) and 956 (s) cm^{-1} are not existing in the spectrum of the free ligand. These two frequency values are assigned to the N-O stretching vibrations of the nitrate group coordinated with the Ag atom. The other N-O stretching vibration for the nitrate group was observed at 1196 (w) cm^{-1}. These stretching vibrations corresponding to experimental values were calculated at 1364, 1184/1186/1190, and 957 cm^{-1}, respectively.

In a study found in the literature, the silver nitrate complex of the 3-bromoquinoline molecule ($[Ag(3BrQ)_2NO_3]$) was synthesized, and its spectroscopic characterization was performed. In this study, N-O stretching vibrations of the nitrate group were observed at 1579, 1382, and 1057 cm^{-1} and calculated at 1583, 1371, and 1058 cm^{-1} [43]. In another study, the silver nitrate complex of the indazole molecule was synthesized, and it was reported that the N-O stretching vibration of the nitrate group was observed at 1355 cm^{-1} and calculated at 1372 cm^{-1} [44].

In another study, it was reported that the two peaks observed at 1516 and 1361 cm^{-1} in the recorded IR spectrum of the synthesized 1,3-benzenedimethanaminium bis(trioxonitrate) molecule were assigned to the N-O stretching vibrations of the nitrate group [15]

In the synthesized complex, the C=N stretching vibration was observed at 1583 (vs) cm^{-1}, and the C-O stretching vibration for the hydroxy group was observed at 1285 (s) cm^{-1}. These two vibration values for the free ligand were observed at 1565 (w) and 1275 (s) cm^{-1}, respectively. The 18 cm^{-1} shift in the C=N stretching vibration and the 10 cm^{-1} shift in the C-O stretching vibration show that the Ag atom is coordinated with the N and O atoms of the free ligand. Additionally, another C=N stretching vibration was recorded at 1457 (m) cm^{-1} and calculated at 1441 cm^{-1}. C-N stretching vibration is observed together with C-C stretching vibration at 1344 (vc) cm^{-1} in the experimental IR spectrum. The theoretical value corresponding to this vibration value was determined as 1339/1341 cm^{-1}.

The C-C stretching vibration for the ring attached to the hydroxy group of the synthesized complex was observed at 1589 cm^{-1}, while this vibration value was observed at 1615 (m) cm^{-1} for the free ligand. According to this result, it is clear that the Ag atom and the oxygen atom of the hydroxy group are coordinated, and as a result, a shift occurs in the C-C stretching vibrations in the ring. Also, the C-C stretching vibrations of the rings of the ligands in the synthesized complex were observed as 1478 (m), 1344 (vs), and 1225 (s) cm^{-1}. Theoretical results corresponding to these experimental values were obtained at 1488 and 1236 cm^{-1}.

The C=N, C-N, C-C and C-O vibrations are observed in the regions

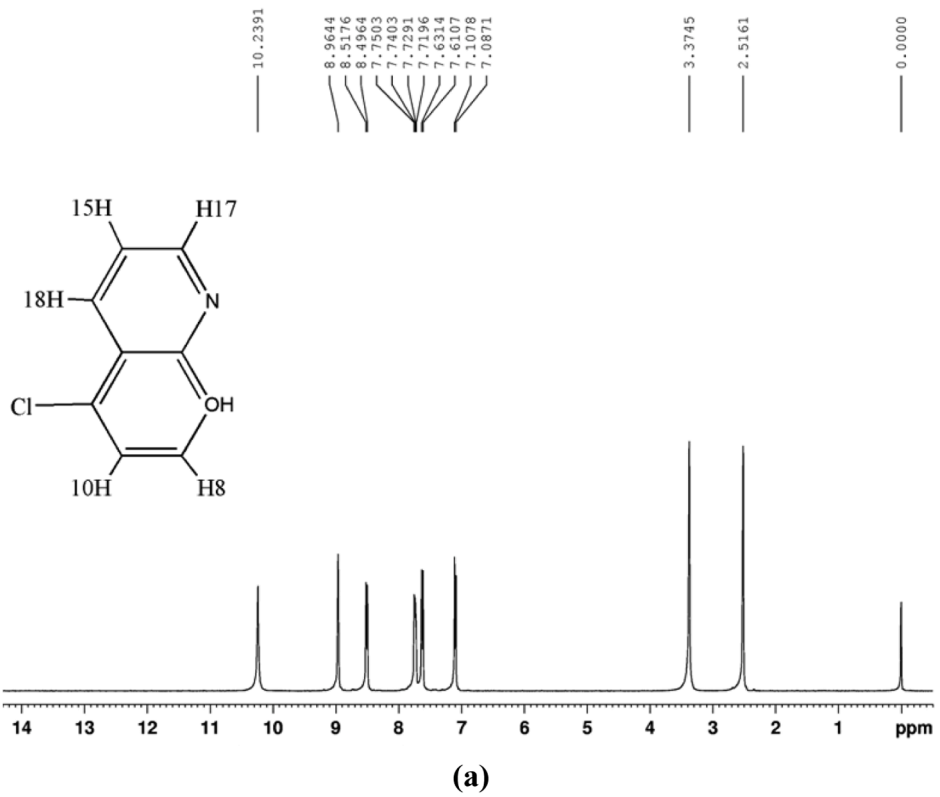

(a)

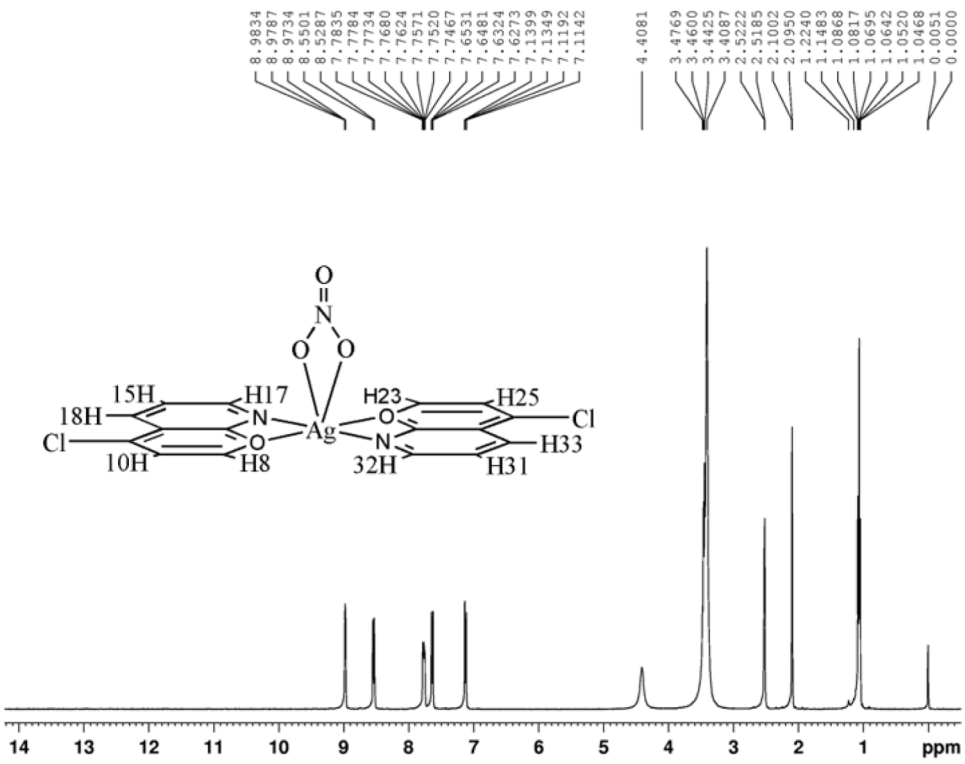

(b)

Fig. 2. Experimental ^{1}H NMR spectra of 5Cl8HQ molecule (a) and the $[Ag(C_9H_5ClNO)_2NO_3]$ complex (b).

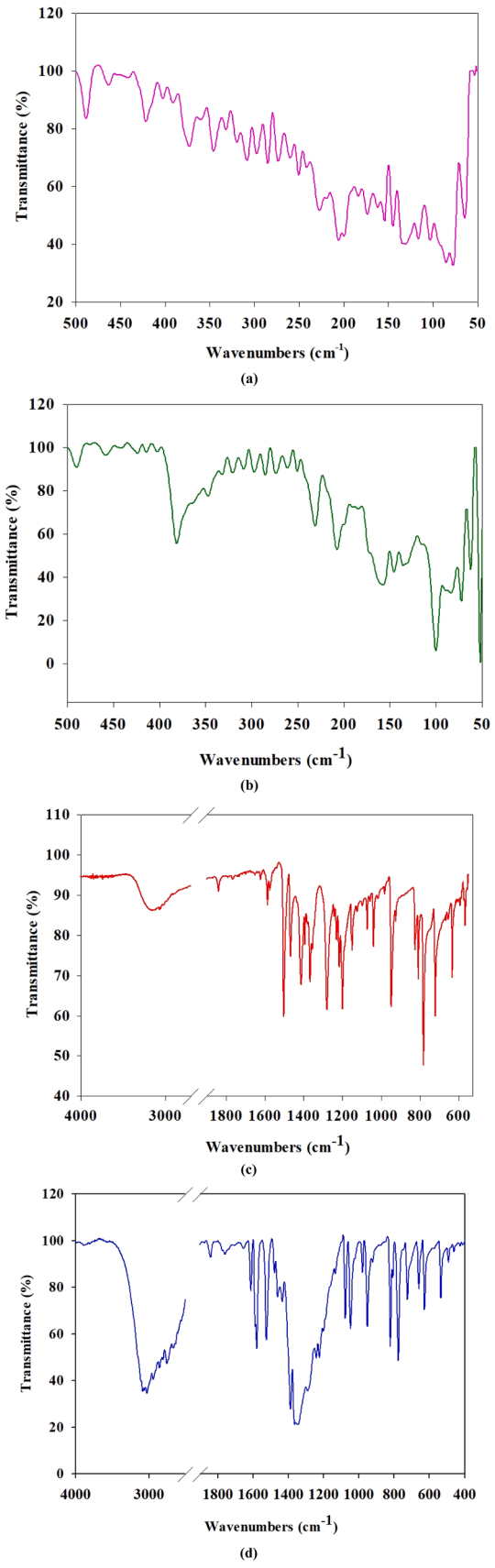

Fig. 3. Experimental Far-IR and FT-IR spectra of the 5Cl8HQ molecule and the synthesized $[Ag(C_9H_5ClNO)_2NO_3]$ complex.

Table 2
Comparison of the observed and calculated vibrational spectra, their detailed assignments and total energy distribution of the $[Ag(C_9H_5ClNO)_2NO_3]$ complex.

Calculated		Observed			
Mode	Fre	I_{IR}[a]	Ligand IR	Complex IR	TED[b]
1	17	0.18			$17\delta_{NAgN} + 11\Gamma_{CCCC} + 24\Gamma_{NAgNC} + 13\Gamma_{NAgNO}$
2	19	0.33			$12\Gamma_{NAgNO} + 43\Gamma_{AgNCC}$
3	33	0.50			$44\Gamma_{ONOAg} + 26\Gamma_{CNAgN}$
4	39	0.23			$19\Gamma_{ONOAg} + 44\Gamma_{CNAgN}$
5/6	43	0.09			$11\delta_{NON} + 40\Gamma_{NAgNO} + 19\Gamma_{ONOAg}$
7	69	1.37		62m	$55\Gamma_{ONOAg}$
8	78	3.59	77 s	72 s	$10\upsilon_{AgO} + 25\delta_{NON} + 20\delta_{OAgO}$
9	86	3.01	84 s		$15\upsilon_{AgO} + 21\delta_{NON} + 12\Gamma_{CCCC}$
10	97	1.81		100 vs	$12\delta_{NAgN} + 40\Gamma_{CCCC} + 11\Gamma_{CCCO}$
11	115	3.81	117 s	136 m	$65\upsilon_{AgN}$
12	144	4.14	144 s	145 m	$56\delta_{OAgO} + 11\Gamma_{CCCN} + 15\Gamma_{CCCC}$
13	161	3.23	154 s	159 s	$56\upsilon_{AgO} + 10\Gamma_{CCNC}$
14	173	5.00	173 s		$12\delta_{AgNC} + 10\Gamma_{CCCN} + 11\Gamma_{CCCC}$
15	179	0.47			$13\Gamma_{CCCN} + 15\Gamma_{CCNAg}$
16	181	2.17			$12\delta_{AgNC} + 11\Gamma_{CCCC} + 12\Gamma_{CCNC}$
17	198	1.06	199 vs		$13\Gamma_{CCCN} + 15\Gamma_{OCCC}$
18	200	1.07			$45\delta_{OAgO}$
19	204	5.26	206 vs	208 m	$21\delta_{ClCC} + 12\Gamma_{CCNAg} + 15\Gamma_{CCCN}$
20	218	1.48			$39\delta_{NAgN} + 23\Gamma_{CCNAg}$
21	225	7.20	227 s	232 m	$39\delta_{CCN}$
22	278	4.88			$25\upsilon_{AgN} + 14\upsilon_{ClC}$
23	298	0.62			$31\upsilon_{AgN} + 35\Gamma_{CNAgN}$
24	313	3.79			$35\Gamma_{ClCCC}$
25	317	8.21			$62\Gamma_{OCCC}$
26	382	5.16	373 m	382 m	$45\upsilon_{ClC} + 11\delta_{CCC}$
27	404	0.12			$39\upsilon_{ClC} + 12\delta_{ClCC}$
28	441	1.15			$10\delta_{CNAg} + 37\delta_{ClCC}$
29	454	0.28			$10\Gamma_{CCCN} + 16\Gamma_{CAgCN}$
30	465	0.17		465 vw	$10\delta_{CCN} + 10\delta_{OCC} + 10\delta_{ClCC} + 18\Gamma_{CCNAg}$
31	468	1.98			$27\Gamma_{CCCC} + 32\Gamma_{CCNAg}$
32/33	486	0.14	488m	491 w	$32\Gamma_{CCCC}$
34	506	0.05			$10\delta_{CCN}$
35	515	2.30			$14\delta_{CCN}$
36	544	1.57			$10\delta_{OCC}$
37	555	14.20	569 m	534 m	$10\upsilon_{AgN} + 10\upsilon_{AgO} + 10\delta_{CCC}$
38/39	608/611	3.39	596 w		$26\Gamma_{CCCC} + 12\Gamma_{CCNC}$
40	626	0.01			$51\delta_{OCC}$
41/42	636/641	6.44		628 m	$10\upsilon_{AgO} + 81\delta_{ONO}$
43/44	647/652	4.81	637 s	658 m	$14\Gamma_{CCCN} + 27\Gamma_{CCNC}$
45	661	3.68			$32\delta_{OCC}$
46	670	0.83			$18\upsilon_{ClC} + 11\delta_{CCC}$
47	680	34.18			$14\upsilon_{ClC} + 20\delta_{CCC} + 12\delta_{OCC}$
48	721	7.73	725 s	725 m	$99\Gamma_{OOON}$
49	745	4.54			$24\delta_{CCC}$
50	756	17.33	787 vs	777 s	$29\delta_{CCC}$
51/52	799/802	7.82	812 s	807 m	$25\Gamma_{CCCH} + 27\Gamma_{ClCCC}$
53/54	828	1.90	831m	822 vs	$65\delta_{CCC}$
55/56	856	3.25			$53\Gamma_{CCCH}$
57/58	863	35.25			$63\Gamma_{CCCH} + 10\Gamma_{ClCCC}$
59	957	6.26		956 s	$87\upsilon_{ON}$
60/61	962/970	16.53	945 vs		$10\upsilon_{ClC} + 27\delta_{CCN}$
62/63	984	0.05	982 w	984 m	$79\Gamma_{CCCH}$
64/65	1000	0.23			$84\Gamma_{HCCN}$
66/67	1041	6.48	1044 m	1046 s	$63\Gamma_{HCCN} + 23\Gamma_{CCCN}$
68/69	1058/1060	24.70	1074 m	1077 s	$45\upsilon_{CC}$

(*continued on next page*)

Table 2 (*continued*)

Calculated		Observed			
Mode	Fre	I_{IR}[a]	Ligand IR	Complex IR	TED[b]
70/71	1098	6.27	1095 w		$10\upsilon_{CO} + 45\upsilon_{CN} + 11\delta_{CCH} + 10\delta_{CCC}$
72/73	1151	1.56	1147 m		$15\upsilon_{CC} + 18\delta_{CCH}$
74/ 75/ 76	1184/ 1186/ 1190	45.95	1202 vs	1196 w	$45\upsilon_{ON}$
77/78	1236	17.64	1223 s	1225 s	$15\upsilon_{CC} + 10\upsilon_{CN} + 35\delta_{CCH}$
79/80	1260	20.48	1235 m	1242 s	$15\delta_{CCH}$
81/82	1283	76.17	1275 s	1285 s	$10\upsilon_{CC} + 16\upsilon_{CO} + 13\delta_{CCH}$
83/84	1339/ 1341	17.75		1344 vs	$36\upsilon_{CC} + 14\upsilon_{CN}$
85	1364	100.00		1361vs	$87\upsilon_{ON}$
86	1403/ 1405	89.02	1372 s	1388 vs	$15\delta_{CCH}$
88/89	1429/ 1431	6.30	1415 s	1434 m	$46\delta_{CCH}$
90	1437	1.28			$14\upsilon_{CC} + 10\delta_{CCH}$
91	1441	11.06		1457 m	$44\upsilon_{CN} + 10\delta_{CCH}$
92/93	1488	77.82	1467 m	1478 m	$17\upsilon_{CC} + 22\delta_{CCH}$
94/95	1530	42.49	1507 s	1523 vs	$21\upsilon_{CC}$
96/97	1608	8.24	1565 w	1583 vs	$33\upsilon_{CN} + 15\upsilon_{CC}$
98/99	1617	9.34	1589 w	1615 s	$33\upsilon_{CC} + 24\delta_{CCC}$
100/ 101	1641	3.28			$44\upsilon_{CC}$
102/ 103	3231	1.65	3069 m	3088 vs	$98\upsilon_{CH}$
104/ 105	3232	0.91			$96\upsilon_{CH}$
106/ 107	3240	0.24			$98\upsilon_{CH}$
108/ 109	3250	0.60			$96\upsilon_{CH}$
110/ 111	3258	1.74			$98\upsilon_{CH}$

υ: stretching, δ: in-plane bending, Γ: torsion, s: strong, m: medium, w: weak, v: very.

[a] Relative absorption intensities and relative Raman intensities normalized with highest peak absorption equal to 100.

[b] Total energy distribution level (TED) less than 10% are not shown.

1672-1566 [45], 1382-1266, 1650-1200 [46], and 1260-1000 cm^{-1} [47], respectively. Although a shift is observed in the frequency values of the synthesized $[Ag(C_9H_5ClNO)_2NO_3]$ complex compared to those of the ligand, they are compatible with the ranges in the literature.

When the Far-IR and FT-IR spectra recorded for the $[Ag(C_9H_5ClNO)_2NO_3]$ complex were examined, Ag-N stretching vibrations were observed at 136 (m) and 534 (m) cm^{-1}. Theoretical Ag-N stretching vibrations corresponding to these experimental values were calculated at 115 and 555 cm^{-1}. In addition, data were also obtained for this stretching vibration at 298 and 278 cm^{-1} in theoretical calculations. N-Ag-N in-plane bending vibration was observed at 100 (vs) cm and calculated at 97 cm^{-1}. The Ag-N stretching vibrations for the synthesized silver nitrate complex of 4-pyridinecarboxaldehyde were observed at 645, 137, 90, and 76 cm^{-1} [48].

Ag-$O_{nitrate}$ stretching vibrations of the title complex were observed at 628 (m), 534 (m), 159 (s), and 72 (s) cm^{-1} and calculated at 636/641, 569, 161, and 78 cm^{-1}. While the Ag-$O_{nitrate}$ vibrations of the synthesized silver nitrate complex of 2-methylquinoxaline were measured at 640 (vw, IR), 643 (w, Ra), 124 (vw/IR), 123 (m, Ra), and 100 (w, IR) cm^{-1}, this vibration frequency was found at 649, 261, 126, and 101 cm^{-1} in DFT calculations [49]. In another study, it was reported that the Ag-$O_{nitrate}$ stretching vibration was observed at 642 cm^{-1} in the IR spectrum for the synthesized $[Ag(3\text{-}Py\text{-}CHO)_2NO_3]$ complex [50].

The correlation graph drawn to show the harmony between the experimental and theoretical frequency values of the synthesized Ag(I) complex is presented in supplementary Fig. S2. The R^2 value was found to be 0.999. The obtained R^2 value shows that the experimental and theoretical frequency values are quite compatible with each other. a) Far-IR of C_9H_6ClNO (5Cl8HQ) molecule, b) Far-IR of $[Ag(C_9H_5ClNO)_2NO_3]$ complex c) FT-IR of C_9H_6ClNO (5Cl8HQ) molecule, d) FT-IR of $[Ag(C_9H_5ClNO)_2NO_3]$ complex

3.4. HOMO-LUMO molecular orbital analysis

The highest energy molecular orbital occupied by electrons (HOMO) and the lowest energy molecular orbital unoccupied by electrons (LUMO) represent the ability to donate and gain electrons from a compound, respectively [51]. The energy gap between these molecular orbitals is used to evaluate the chemical reactivity and kinetic stability of a compound. That is, the energy values of HOMO – LUMO orbitals play an important role in determining the chemical hardness or chemical softness of the molecular system [52]. Molecules with a high HOMO-LUMO energy gap are considered rigid and have low polarization. In contrast, soft molecules have a low HOMO-LUMO energy gap and high polarization [53]. The HOMO and LUMO energy values of the synthesized $[Ag(C_9H_5ClNO)_2NO_3]$ complex were calculated using the B3LYP functional with the SDD basis set in the DFT method [54]. In addition, after calculating the energy values of HOMO and LUMO orbitals, the energy values of other quantum chemical properties were calculated with the following equations [55]:

$$I = -E_{HOMO}\ (\text{ionization potantial}) \tag{5}$$

$$A = -E_{LUMO}\ (\text{electron affinity}) \tag{6}$$

$$\eta = (-E_{HOMO} + E_{LUMO})/2\ (\text{global hardness}) \tag{7}$$

$$\mu_c = (E_{HOMO} + E_{LUMO})/2\ (\text{chemical potential}) \tag{8}$$

$$\chi = -\mu_c\ (\text{electronegativity}) \tag{9}$$

$$\sigma = 1/\eta\ (\textit{global softnes}) \tag{10}$$

$$\omega = \mu_c^2/2\eta\ (\text{global electrophilicity}) \tag{11}$$

The energy values obtained are presented in Table 3. The HOMO and LUMO energy values for the synthesized title complex were calculated to be -5.95 and -4.86 eV, and the energy gap between these two orbitals was found to be 1.08 eV. The energy gap has been linked to a variety of biological features, including antibacterial, antioxidant, antidiabetic, and DNA binding properties [4]. The synthesized $[Ag(C_9H_5ClNO)_2NO_3]$ complex has a stable structure due to the negative energy values of its HOMO and LUMO orbitals [56,57]. The fact that the chemical potential value of the title complex is negative means that this compound is stable [58]. For this reason, they cannot spontaneously decompose into their elements. In addition, the global hardness value was calculated as 0.54 eV, respectively. In a previous study, the energy gap value for the 5-chloro-8-hydoxyquinoline ligand used in the synthesis of the title molecule was found to be 2.52 eV, and its global hardness value was 1.48 eV [59]. According to this result, we can say that the synthesized complex is more reactive than the free ligand.

Fig. 4 presents the charge distributions of HOMO and LUMO molecular orbitals. When the green color symbolizes the negative phase, the red color represents the positive phase [51]. When the charge distribution for the HOMO orbital is examined, it can be seen that the electron density is distributed, especially on the nitrogen (N) and oxygen (O) atoms in the nitrate group. When the electrons from the HOMO orbital were moved to the LUMO orbital as a result of excitation, it was determined that the electrons were distributed on the part where the pyridine rings and the hydroxy groups attached to the benzene ring

Table 3
The energy values of the quantum chemical properties of the $[Ag(C_9H_5ClNO)_2NO_3]$ complex.

Molecular Orbitals	Energy (eV)		Energy gap (eV)	Ionization potential (I) (eV)	Electron affinity (A) (eV)	Global hardness (η) (eV)	Electronegativity (χ) (eV)	Chemical potential (μ_c) (eV)	Global softness (σ) (eV^{-1})	Global electrophilicity (ω) (eV)
H	-5.95	ΔE_{H-L}	1.08	5.95	4.86	0.54	5.40	-5.40	1.84	26.93
L	-4.86									
H-1	-6.42	$\Delta E_{H_{-1}-L_{+1}}$	0.48	6.42	5.95	0.24	6.18	-6.18	4.19	80.17
L+1	-5.95									
H-2	-6.58	$\Delta E_{H_{-2}-L_{+2}}$	3.74	6.58	2.84	1.87	4.71	-4.71	0.54	5.94
L+2	-2.84									

H: HOMO, L: LUMO

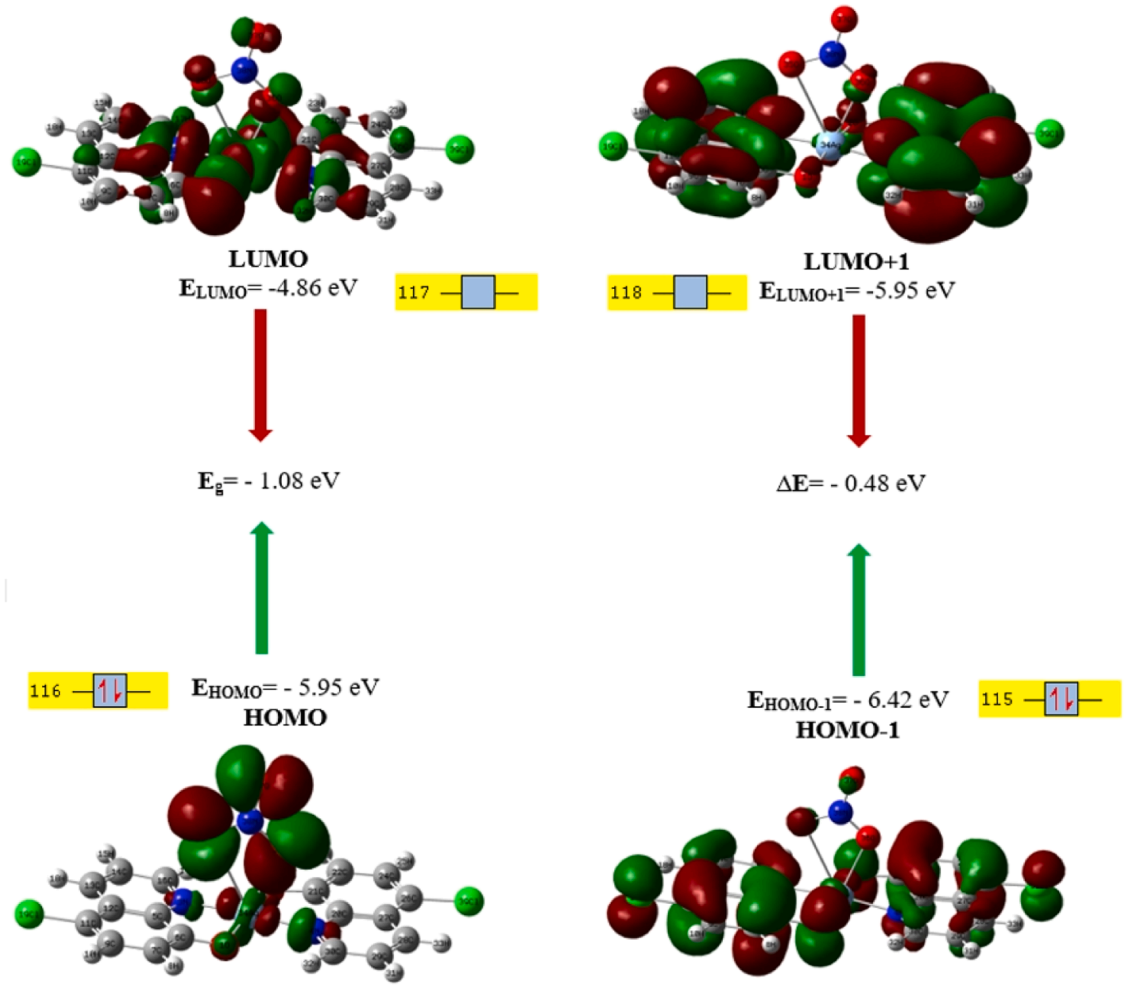

Fig. 4. HOMO-LUMO moleculat orbital distribution of the $[Ag(C_9H_5ClNO)_2NO_3]$ complex.

bonded with the silver atom.

3.5. UV-Vis spectrum analysis

The formation of the complex was confirmed by recording the UV-Vis spectra of the 5CL8HQ (C_9H_6ClNO) molecule and the synthesized $[Ag(C_9H_5ClNO)_2NO_3]$ complex. For both structures, electronic absorption spectra were recorded from 190 to 1100 nm in the ethanol solvent. The absorption band of the 5CL8HQ molecule was observed at 328 nm. The band obtained for the free ligand was slightly shifted to a longer wavelength (batochromic shift) due to complex formation (ligand metal charge transfer) and was observed at 340 nm. Experimental UV-Vis absorption spectra are presented in Fig. 5. The reason for this shift is that the experimental results were obtained for bulk material while the theoretical calculations were performed using optimized geometry. Additionally, calculated wavelengths, excitation energies, oscillator power, and major contributions are given in Table 4 with the experimental wavelength. While absorption bands for the 5CL8HQ molecule were calculated at 311, 241, and 185 nm, two absorption bands were calculated at 359 and 270 nm for the synthesized title complex. The absorption band observed at 311 nm due to the HOMO/LUMO transition for the 5CL8HQ molecule was observed at 328 nm in the experimental spectrum. For the $[Ag(C_9H_5ClNO)_2NO_3]$ complex, the band calculated due to the HOMO/LUMO+1 and HOMO/LUMO+2 transitions at 359 nm was observed at 340 nm. According to the obtained results, the experimental and theoretical wavelengths for the absorption bands of both the

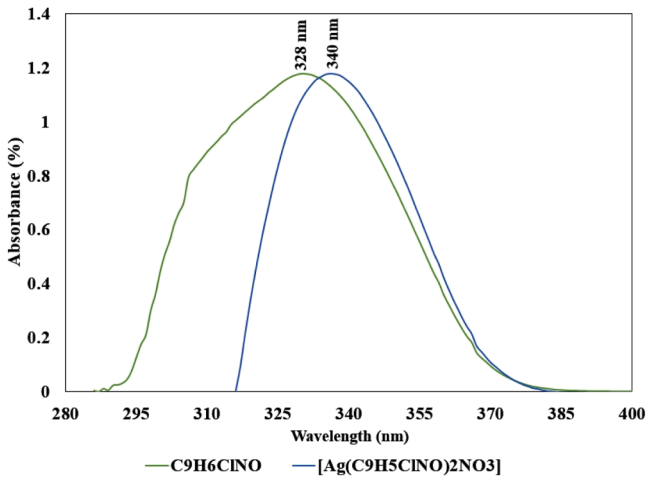

Fig. 5. Experimental UV-Vis spectra of the C_9H_5ClNO (5CL8HQ) molecule and $[Ag(C_9H_5ClNO)_2NO_3]$ complex.

free molecule and the complex are in agreement.

3.6. Molecular electrostatic potential surface map (MEP) analysis

The MEP obtained as a result of DFT calculations are quite useful to predict the relative reactivity positions of a molecule for electrophilic and nucleophilic attacks [60,61]. On the designed map surface, different values of the electrostatic potential are represented by different colors. Red represents regions with the most electronegative potential, while blue represents regions with the most positive electrostatic potential [62]. Green represents a region with zero potential. The yellow color represents slightly electron-rich regions [63,64]. The color code in the MEP map of the synthesized complex presented in Fig. 6 was calculated between −6.517e−2 a.u. and +6.517e−2 a.u. When the map designed for the $[Ag(C_9H_5ClNO)_2NO_3]$ complex is examined, the red-colored region (the electrophilic region) concentrates on the O atoms of the nitrate group. In previous studies in the literature, MEP maps of synthesized silver nitrate complexes were investigated, and in these studies, it was reported that the most negative (electrophilic) regions were distributed around the oxygen atoms of the nitrate group [65]. In other words, this region has the most negative value and is the site of nucleophilic attack during the chemical reaction. The N and O atoms in the structure, coordinated with the silver atom of the free ligands, are in the yellow region. Additionally, the Cl atoms of the ligands are in the yellow region. For this reason, these atoms are also in the slightly electron-rich region.

3.7. Fukui function analysis

One of the other methods used to determine the electrophilic and nucleophilic regions of the molecule is estimated by calculating Fukui functions [66,67]. Using a finite difference methodology, Fukui functions are calculated from the Hirshfeld charges of the neutral, cationic, and anionic states of the synthesized complex with the following equations:

$$f_k^{\,0} = (1/2)[q_k(N+1) - q_k(N-1)] \tag{12}$$

$$f_k^{\,-} = q_k(N) - q_k(N-1) \tag{13}$$

$$f_k^{\,+} = q_k(N+1) - q_k(N) \tag{14}$$

While $f_k^{\,+}$ and $f_k^{\,-}$ in the equations are defined as the nucleophilic and electrophilic indices of the synthesized complex, respectively, $f_k^{\,0}$ is defined as the neutral attack index. Additionally, qk in these equations is represented as the electron population in the rth atom. qkN, qk(N+1), and qk(N-1) are the total charge amounts in the neutral, anionic, and cationic states of the title complex [68]. In many studies in the literature, $\Delta f(r)$ defined by the following equation, called a dual descriptor, is used to ensure a clear distinction between electrophilic and nucleophilic regions.

$$\Delta f(r) = f^{+}(r) - f^{-}(r) \tag{15}$$

If the $\Delta f(r)$ value obtained from this equation is greater than zero, that atom is attractive for nucleophilic attack; that is, it is electrophilic. If the $\Delta f(r)$value is less than zero, that atom is attractive for electrophilic attack; that is, it is nucleophilic [69].

The Fukui function values of the $[Ag(C_9H_5ClNO)_2NO_3]$ complex were listed in supplementary Table S2, and graphical representations of the dual descriptors created by using the Multiwfn program were also presented in Fig. 7. The blue areas indicate negative (electrophilic) atoms, and the green areas indicate positive (nucleophilic) atoms. When Fig. 7 is examined, the oxygen atoms of the nitrate group (O_{35}, O_{36}, and

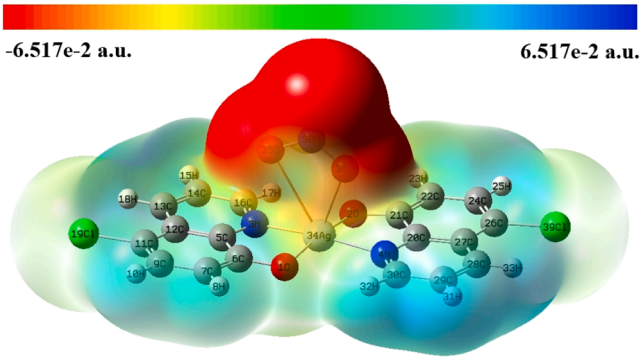

Fig. 6. Molecular electrostatic potential surface map of the [Ag $(C_9H_5ClNO)_2NO_3$] complex.

Table 4
Experimental and theoretical UV–Vis wavelength (λ), band gap energy (eV), oscillator strength, and major contributions of the (5CL8HQ) molecule and [Ag $(C_9H_5ClNO)_2NO_3$] complex.

Molecule	Experimental	Theoretical				
	λ (nm)	λ (nm)	E (eV)	f	Symmetry	Major Contributions
$[Ag(C_9H_5ClNO)_2NO_3]$	340	359	3.45	0.4925	Singlet-A	HOMO → LUMO+1 HOMO-1 → LUMO+2
		270	4.59	0.6553	Singlet-A	HOMO → LUMO+1 HOMO-1 → LUMO+2
5CL8HQ	328	311	3.98	0.1920	Singlet-A	HOMO → LUMO
		241	5.15	1.2106	Singlet-A	HOMO-1 → LUMO
		185	6.72	0.3173	Singlet-A	HOMO-4 → LUMO+1 HOMO-3 → LUMO+1

λ:wavelengths, E: Energy, *f*:oscillator strengths.

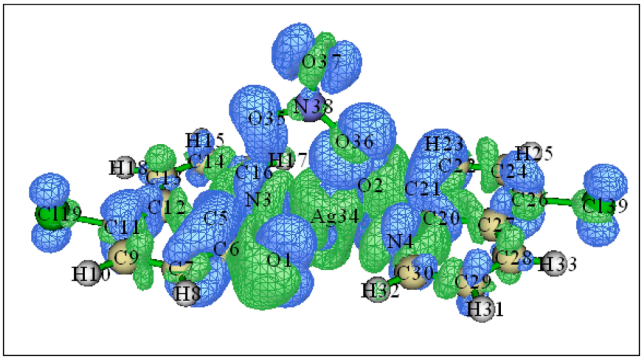

Fig. 7. Dual descriptor image of the $[Ag(C_9H_5ClNO)_2NO_3]$ complex.

O_{37}) are in the blue region. Additionally, C_5, C_{11}, C_{14}, C_{21}, C_{22}, and C_{29} atoms are also located in the blue region. For this reason, these atoms have negative charge values and exhibit electrophilic behavior. The dual descriptor image created using the Multiwfn package program and presented in Fig. 7 was compared with the dual descriptor results obtained from Gaussian calculations, and it was determined that they were compatible with each other. In the results obtained from Gaussian calculations, it was determined that the most electrophilic atom was the oxygen atom of the nitrate atom, and the most nucleophilic atom was the silver atom. In addition, the results obtained for Fukui functions also support the data obtained from the MEP map.

3.8. Charge analysis

The electronic charge distribution in a molecule has a significant effect on the vibrational spectra [52]. It is also one of the important computational methods used to predict the electrophilic and nucleophilic sites of the molecule during a chemical reaction. Therefore, the NBO, atomic polar tensor (APT), and Hirshfeld charges for the optimized structure of the title complex were calculated. The obtained results are presented in supplementary Table S3 and Fig. 8.

According to the results of all three charge analyses, the most negative atoms of the $[Ag(C_9H_5ClNO)_2NO_3]$ complex were found to be O1, O2, N3, N4 atoms, and O35, O36, and O37 atoms of the nitrate group. The atoms with the most positive values were found to be the Ag atom and the nitrogen atom (N38) of the nitrate group. When these results are compared with the MEP map, it is possible to see that there is harmony between them. Similarly, it was stated that the atoms with the most negative values in the MEP map were the oxygen atoms of the nitrate group, and the O1, O2, N3 and, N4 atoms were slightly rich in electrons. Additionally, it was determined that the charge analysis results and the Fukui function data were quite compatible.

3.9. Topology analyses

3.9.1. ELF and LOL analyses

ELF and LOL are tools that apply covalent bond analysis to identify chemical properties of a molecule, such as molecular bonding, chemical shell structure, and lone pair electrons of compounds [70,71]. Both maps provide information with a color distribution based on the electron density charge. The ELF color map for the title complex was plotted at a scale of 0.0–1.0. The plotted ELF value in the range of 0.5 to 1.0 represents bound and nonbonding localized electrons, while a value below 0.5 indicates regions with non-localized electrons [72]. ELF and LOL maps for the synthesized complex are presented in Fig. 9. When the ELF map is examined, it is seen that the red-colored regions, that is, the bound and unbound localized electrons, are concentrated around the hydrogen atoms of the free ligand in the structure. In addition, the blue rings observed around some C and Cl atoms of the complex represent regions with delocalized electron density. The LOL map is interpreted similarly to the ELF map [73]. In the LOL map, red-colored regions representing bound and unbound localized electrons were observed around H atoms, while blue-colored rings representing delocalized electrons were observed around C, Ag, and Cl atoms in the complex.

3.9.2. RDG and NCI analyses

The NCI analysis proved to be a highly effective method for comprehending the covalent bonds, non-covalent interaction, and the degree of charge transfer present inside the compound [70,74,75]. This

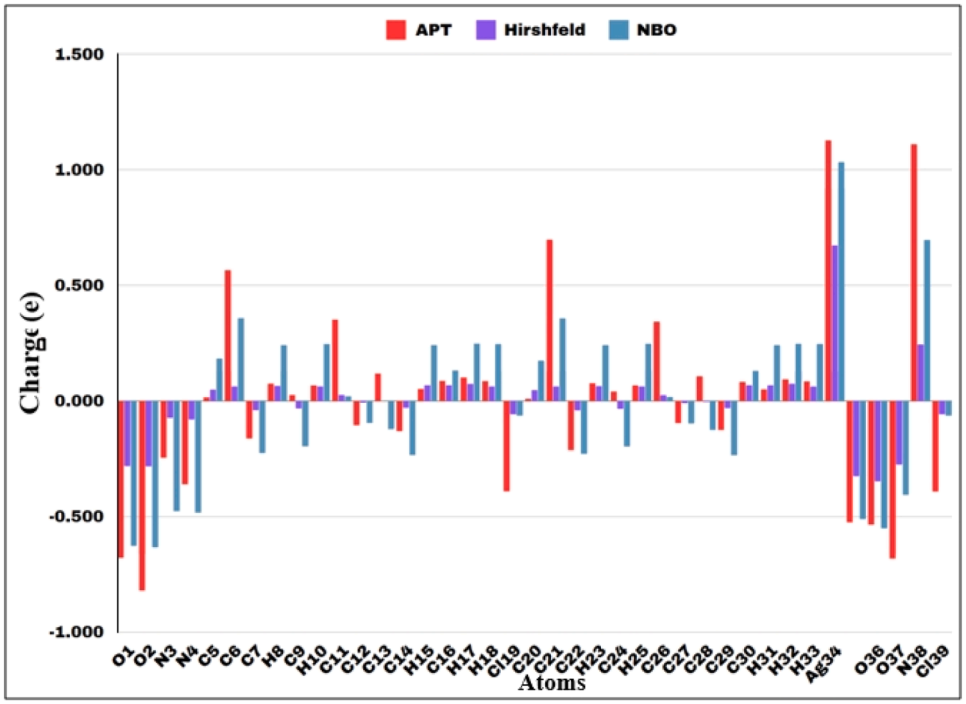

Fig. 8. Apt, NBO, Hrshfeld electron charge distribution of the $[Ag(C_9H_5ClNO)_2NO_3]$ complex.

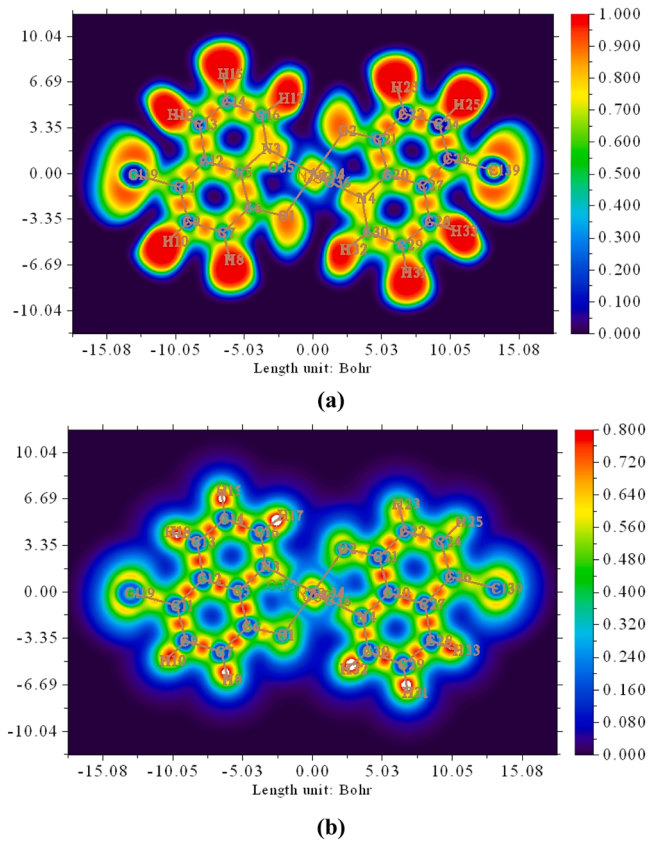

Fig. 9. Color-filled map of ELF (a) and LOL(b) for the [Ag $(C_9H_5ClNO)_2NO_3$] complex.

approach allows for the identification of NCI using RDG isosurfaces, as described by the following relationship [76]. The NCI and RDG were plotted against electron density ($\text{sin}(\lambda_2)\rho$) to investigate the attraction and repulsive forces (Fig. 10). The 3D color scaling of non-covalent interaction shows the solid repulsive effect. The red spheres are at the center of quinoline and benzene rings in free ligand, and the other is shown in the C-O group with an Ag atom. The spikes around +0.02 to +0.05 a.u. represent the steric effect and show $\rho>0$, $\lambda2>0$. Intermolecular C_{16}-H_{17}….O_2 hydrogen bonding interactions are shown by the appearance of green spheres between oxygen and hydrogen atoms, which has been verified using atoms in molecules (AIM) analysis.

3.9.3. QTAIM analysis

AIM analysis used a topological study of electronic density to better understand non-covalent interactions [70]. An interesting tool for determining the strength of the contact is provided by the topological characteristics of a number of intra- and intermolecular connections [77, 78]. Fig. 11 depicts the relationship between the silver (Ag) metal atom and bonds obtained from each bond critical coint (BCPs), while Table 5 provides the topological and geometric parameters of the bonds generated by the interacting atoms. The topological parameters of the bond critical point and Laplacian of electron density $\nabla^2\rho(r)$, kinetic energy G (r), total energy densities H(r), potential energy density V(r), and binding energy (Eint) are summarized in Table 5.

Concerning the BCPs of hydrogen bonds, the C_{16}-H_{17}….O_2 hydrogen bonds were weak with a binding energy 1.07 kJ/mol with $\nabla^2\rho(r) > 0$ and $H(r) > 0$. According to this result, the fact that the Laplace electron density $\nabla^2\rho(r)$ is higher than 0.004 a.u. and the bond critical points $\rho(r)$ are higher than 0.002 a.u indicate the existence of hydrogen bonds [79]. The interaction energy Eint (45.974 kcal/mol) indicates a strong interaction between the Ag atom is coordinated with the N and O atoms of the

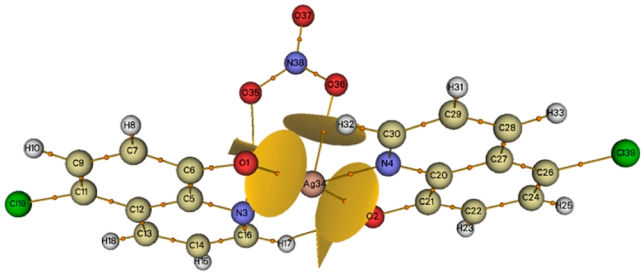

Fig. 11. Graphical representation of the AIM analysis of the [Ag $(C_9H_5ClNO)_2NO_3$] complex.

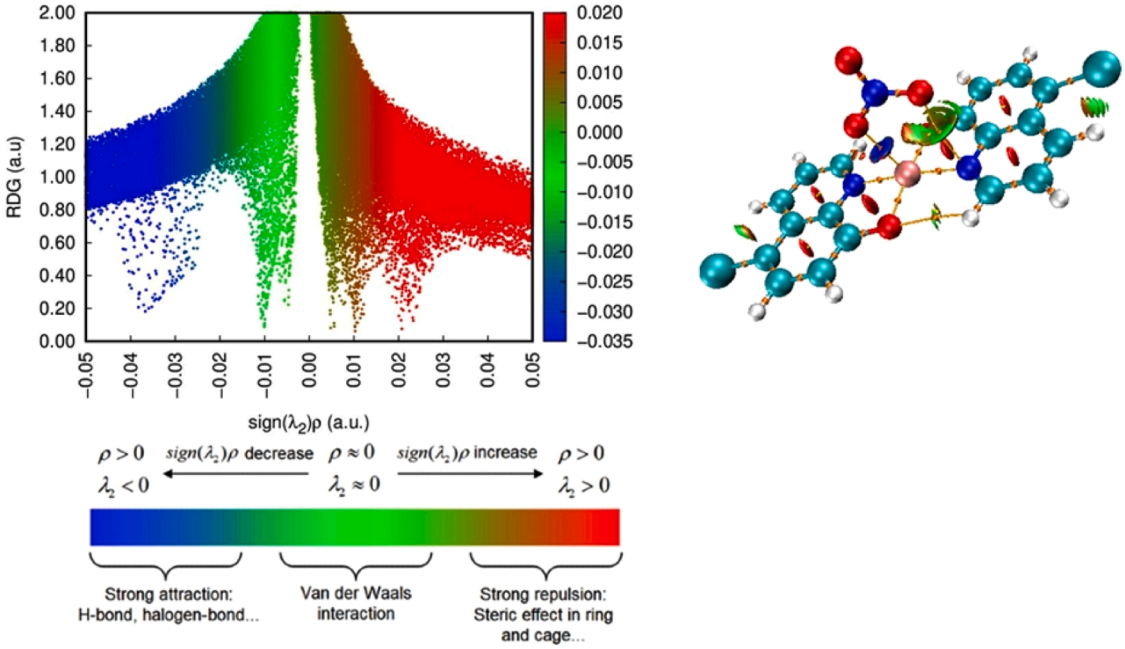

Fig. 10. RDG and isosurface density plots of the [$Ag(C_9H_5ClNO)_2NO_3$] complex.

Table 5
Topological parameters of Ag(I) complex.

Interactions	$\rho(r)$	$\nabla^2\rho(r)$	$H(r)$	$G(r)$	$V(r)$	E_{int}(kcal/mol)	$\|V(r)\|/\ G(r)$
Ag-N_3	0.10388	0.36797	-0.02681	0.11881	-0.14563	43.59	1.22573
Ag-N_4	0.09748	0.35134	-0.02371	0.11155	-0.13527	42.44	1.21262
Ag-O_2	0.10141	0.39854	-0.02262	0.12225	-0.14487	45.45	1.18503
Ag-O_1	0.10161	0.39632	-0.02282	0.12190	-0.14473	45.41	1.18728
Ag….O_{36}	0.03856	0.17272	0.00011	0.04306	-0.04295	13.47	0.99744
N_3….O_{35}	0.01079	0.04284	0.00216	0.00854	-0.00637	1.99	0.74590
C_{16}-H_{17}….O_2	0.00564	0.02945	0.00197	0.00538	-0.00341	1.07	0.63382

D (Å): Distance; ρ(r) (a.u.): Density of electrons; $\nabla^2\rho(r)$ (a.u): Laplacian of electron density; V(r) (a.u): Potential energy density; (Eint) (kcal/mol): Interaction energy

free ligand. We found that the Ag-N and Ag-O bonds exhibit stretching. It was found that $\nabla 2\rho(r) > 0$, $H(r) < 0$ and the ratio $|V(r)|/G(r)$ is 1.2, which were used as descriptives to investigate the nature and strength of these interactions. These findings characterize the closed-shell interactions, including the extremely polar covalent character of the examined bonds. Also, the covalent character of Ag...O and N...O interactions in the silver complex is dominant because it is in the $0.5<|V(r)|/G(r)<1$ condition [80]. According to NBO and RDG investigations, this hydrogen bond interaction is the most powerful and active bioregion in the silver metal complex.

3.9.4. Natural bond orbital (NBO) analysis

The NBO analysis provides information about interactions in both occupied and virtual orbital spaces, and it can improve the analysis of intra- and intermolecular interactions [81]. This method facilitates the examination of charge transfer, delocalization, and conjugative interactions in molecules, as well as the learning of electronic structural aspects and donor-acceptor analysis [14]. The compound's interactions were also confirmed by the NBO analyses, as evidenced by the reduced density gradient (NCI-RDG) isosurfaces. It is a potent instrument for qualitatively comprehending the behavior of electrons within a nucleus system. The B3LYP/SDD level of theory has been utilized to determine the NBO analysis as described in Table 6. Metal-ligand bonding (dative bonding) interactions between a silver ion and a donor atom are thought to be coordination bonds composed of oxygen and nitrogen atoms. The $E^{(2)}$ interaction energies quantitatively study the binding and anti-bonding interactions caused by second-order disturbance. This interaction has led to a transfer of an electron density from the donor atoms LP(O) and LP(N) of the free ligand to the antibonding orbital of LP*(Ag). In the complex, Ag-N (83.04 and 86.54 kcal/mol) interactions are weaker than Ag-O (231.86 and 213.91 kcal/mol) interactions. The highest stabilization energy corresponds to O2→Ag, revealing the intense charge transfer interaction. On the other hand, calculations have shown that interactions with the nitrate anion, Ag...O (12.36 kcal/mol), have lower interaction energies compared to Ag-O1 Ag-O2. The interaction LP(1)(O2)→σ*(C16–H17) with the stabilization energy 1.10 confirms the presence of intermolecular C16–H17…O2 hydrogen bonding interaction. The results are supported by optimized geometry and vibrational analysis.

Table 6
Second-Order perturbation theory analysis of Fock matrix in NBO corresponding to the selected charge transfer interactions of the complex.

Donor (i)→Acceptor(j)	$E^{(2)}(kcal/mol)^a$	$\varepsilon_j - \varepsilon_i(a.u.)^b$	$F(i.\ j)(a.u.)^c$
$LP(1)(N_3)\rightarrow LP^*(5)(Ag)$	86.54	0.06	0.090
$LP(1)(N_4)\rightarrow LP^*(5)(Ag)$	83.04	0.06	0.085
$LP(3)(O_2)\rightarrow LP^*(5)(Ag)$	213.91	0.03	0.098
$LP(3)(O_1)\rightarrow LP^*(5)(Ag)$	231.86	0.03	0.098
$LP(1)(O_{36})\rightarrow LP^*(Ag)$	12.43	0.78	0.090
$LP(1)(O_2)\rightarrow\sigma^*(1)(C_{16}-H_{17})$	1.10	0.45	0.089

σ : sigma bonds, *LP*: lone pairs, LP*: anti-lone pairs
[a]$E^{(2)}$ means energy of hyper conjugative interactions.
[b]Energy difference between donor and acceptor i and j NBO orbitals.
[c]$F_{(i,j)}$ is the Fock matrix element between i and j NBO orbitals

3.10. Antioxidant activity results

3.10.1. In vitro DPPH• and ABTS•+ radical scavenging activity

DPPH• radicals are widely used in antioxidant activity determinations because they interact with lipophilic and hydrophilic antioxidants as well as the weakest antioxidants [82]. The ABTS radical scavenging technique is another way to assess antioxidant levels. ABTS•+ radicals are soluble in both aqueous and inorganic environments. Due to these properties, it has an important place in the evaluation of the antioxidant activities of both lipophilic and hydrophilic substances [83]. In the antioxidant activity determination of the [Ag$(C_9H_5ClNO)_2NO_3$] complex, two different radicals (DPPH• and ABTS•+) inhibitions were determined. The radical inhibition percentages of both this complex and the samples of standard substances (ascorbic acid, BHT) at 25, 50, and 100 μg/mL concentrations were determined. The IC_{50} amounts were then calculated from these percent inhibition values. The findings are presented in Table 7 with Fig. 12.

The quantity of antioxidant substance necessary to reduce the initial radical concentration by 50% is known as the IC_{50} (inhibitory concentration), which demonstrates antiradical activity [84]. A high IC_{50} value indicates low antioxidant activity [85,86]. In this study, the DPPH• radical IC_{50} values of the samples were determined to be complex (97.13 μg/mL), standard ascorbic acid (10.56 μg/mL), and standard BHT (22.64 μg/mL), respectively. Additionally, the ABTS•+ radical IC_{50} values of the samples were determined to be complex (109.04 μg/mL), standard ascorbic acid (14.96 μg/mL), and standard BHT (27.46 μg/mL). From these results, it was determined that the complex had strong radical scavenging and inhibited both radicals. The complex was found to have antioxidant activity when compared to standard substances. It has been determined that this complex, in particular, inhibits the DPPH• radical more strongly. In a study in which cobalt (II) and oxovanadium (IV) complexes were synthesized from quinoline carbaldehyde ligand, the antioxidant capacities of these complexes and the ligand were investigated. The DPPH• radical-scavenging activity of these substances was examined. This study showed that both complexes have greater antioxidant activity than the ligand. Additionally, the IC_{50} values of all samples were calculated and reported as complex 1 (9.15 μg/mL), complex 2 (34.69 μg/mL), and ligand (42.5 μg/mL) [4]. In a study investigating the antioxidant capacity of four complexes produced from 8-hydroxyquinoline, the DPPH• radical-scavenging activities of these substances were determined. The IC_{50} values of the samples were determined as 0.30 mg/mL, 2.97 mg/mL, 10.24 mg/mL, and 15.29 mg/mL [3]. In determining the antioxidant capacities of halogen and nitro derivatives of 8-hydroxyquinoline and copper complexes, the ABTS•+ radical scavenging activities of these substances were investigated. Especially $Cu(BrQ)_2$ has been reported that the complex ($IC_{50} = 33.33 \pm 0.31$ μM) showed stronger ABTS•+ radical inhibition than other complexes. Additionally, it was determined that the ligand of this complex showed higher ($IC_{50} = 8.23 \pm 0.52$ μM) antioxidant properties than the complex [87]. As a result of our study, it can be said that this complex exhibits good antioxidant activity by inhibiting both radicals. In particular, it was observed that the DPPH• radical inhibition of this

Table 7
Radicals inhibition percentages and IC_{50} values of the samples.

Samples	Concentration (μg/mL)	% inhibition ($DPPH^{\bullet}$)	IC_{50} (μg/mL)	% inhibition ($ABTS^{\bullet+}$)	IC_{50} (μg/mL)
$[Ag(C_9H_5ClNO)_2NO_3]$	25	23.62±1.78		20.44±1.69	
	50	38.77±1.59	97.13	35.45±1.49	109.04
	100	49.54±1.56		45.71±1.74	
	25	53.28±1.36		51.32±1.33	
Standard	50	69.44±1.68	10.56	67.22±1.52	14.96
(Ascorbic acid)	100	84.42±2.02		81.33±1.40	
	25	47.21±1.49		45.61±1.51	
Standard (BHT)	50	66.55±1.95	22.64	64.13±2.18	27.46
	100	79.12±1.78		77.36±1.15	

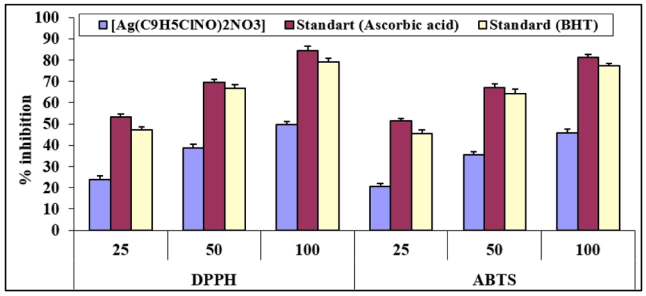

Fig. 12. Inhibition percentages of samples against $DPPH^{\bullet}$ and $ABTS^{\bullet+}$ radicals.

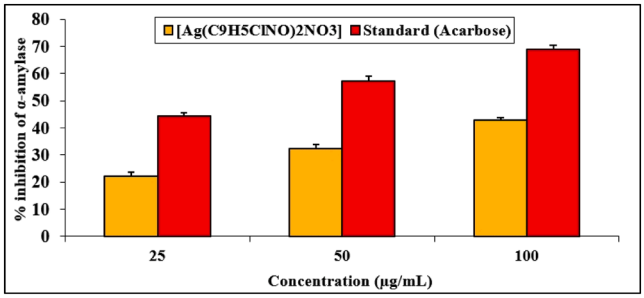

Fig. 13. α-amylase enzyme percentages of the samples.

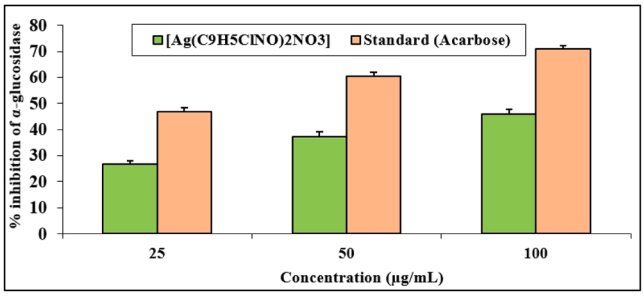

Fig. 14. α-glucosidase enzyme inhibition results.

complex was greater than the $ABTS^{\bullet+}$ radical inhibition. It seems that our antioxidant results are compatible with the literature.

3.11. Antidiabetic activity

3.11.1. In vitro inhibition of α-amylase and α-glucosidase enzymes

Diabetes mellitus is the inability of the pancreas to produce enough insulin, or the insulin produced by the body. It is a metabolic disorder that results from an inability to use it effectively. Chronic diseases caused by diabetes Hyperglycemia (high blood sugar) affects the eyes, kidneys, nerves, heart, and blood vessels. It causes serious damage to many organs of the body, such as [88]. α-amylase inhibitors prevent disorders such as diabetes and obesity. They are also described as very good targets for treatment. These inhibitors delay the breakdown of carbohydrates by creating a suitable environment in the body and increasing satiety. lowers blood sugar [89]. α-Glucosidase, one of the digestive enzymes, is involved in the hydrolysis of carbohydrates into glucose. It is a key enzyme. Inhibition of this enzyme slows carbohydrate synthesis, glucose It delays its release, and thus hyperglycemia is suppressed [90]. Recent studies have focused on the discovery of new α-amylase and α-glucosidase inhibitors. Both the α-amylase enzyme inhibition percentages and IC_{50} values and the α-glucosidase enzyme inhibition percentages and IC_{50} values of the $[Ag(C_9H_5ClNO)_2NO_3]$ complex and standard acarbose in this study are shown in Table 8 and Figs. 13, and 14.

The inhibition percentages of both α-amylase and α-glucosidase enzymes in samples of $[Ag(C_9H_5ClNO)_2NO_3]$ complex and standard acarbose at 25, 50, and 100 μg/mL concentrations were determined. IC_{50} (inhibitory concentration) values were calculated from these percent inhibition results. The α-amylase enzyme IC_{50} values of the complex and standard substance acarbose were determined to be 124.62 and 36.34 μg/mL, respectively. Additionally, α-glucosidase enzyme IC_{50} values were determined to be 113.06 and 27.35 μg/mL, respectively. It was determined that the complex's inhibition of the α-glucosidase enzyme was greater than its inhibition of the α-amylase enzyme (Figs. 13, 14).

In a study investigating the antidiabetic activity of 8-Hydroxyquinolinium 3,5-Dinitrobenzoate, it was reported that the α-amylase enzyme percent inhibition value of this substance at 125 μg/ml concentration was 66.33, while that of standard acarbose was 75.55 [91]. In this study,

Table 8
Inhibition percentages and IC_{50} values of both enzymes of the samples.

Samples	Concentration (μg/mL)	α-amylase % inhibition	IC_{50} (μg/mL)	α- glucosidase % inhibition	IC_{50} (μg/mL)
$[Ag(C_9H_5ClNO)_2NO_3]$	25	22.11±1.55	124.62	26.83±1.22	113.06
	50	32.31±1.56		37.39±1.85	
	100	42.86±1.02		45.93±1.86	
	25	44.34±1.19	36.34	46.91±1.35	27.35
Standard (Acarbose)	50	57.42±1.61		60.44±1.52	
	100	68.97±1.40		70.88±1.28	

100 μg/ml The percent inhibition value of the $[Ag(C_9H_5ClNO)_2NO_3]$ complex α-amylase enzyme at the concentration was determined to be 42.86±1.02 μg/ml, and that of standard acarbose was 68.97±1.40 μg/ml. Additionally, in another study, α-amylase and α-glucosidase enzyme inhibitions of 2-Hydroxyquinoline and its analogues. It has been reported that the IC_{50} values of the α-amylase enzyme at a concentration of 1.000 μg/mL are 2-hydroxyquinoline (130.5±2.2 μg/mL) and 2-methyl-8-hydroxyquinoline analogue (215.4±1.4 μg/mL). It has also been reported that the IC_{50} values of the α-glucosidase enzyme at the same concentration are 2-hydroxyquinoline (64.4±1.7 μg/mL) and 2-methyl-8-hydroxyquinoline analogue (90.7±2.5 μg/mL) [8]. In another study, the antidiabetic activities of 4-hydroxyquinolinone-hydrazones and their derivatives were investigated using the α-glucosidase enzyme. As a result of the study, it was reported that the α-glucosidase enzyme IC_{50} values of these substances varied between 93.5±0.6 and 575.6±0.4 μM. It has also been emphasized that 4-hydroxyquinolinone--hydrazone derivatives are α-glycosidase enzyme inhibitors [10]. It is observed that the study results are compatible.

3.12. Molecular docking analysis

Molecular docking is a crucial method in structure-based drug development because it predicts the interactions and connections between ligands and their target proteins [92]. Molecular docking is an important method where molecules get both fast and reliable results before experimental procedures for cancer disease. It has been determined that these radicals formed as a result of oxidative stress cause many diseases, such as diabetes, asthma, cancer, hypertension, cardiovascular diseases, pneumonia, hepatitis, and inflammatory diseases [93]. Molecular docking is an important method where molecules get both fast and reliable results before experimental procedures for oxidative stress cause diseases. Thanks to antioxidant systems, the harmful effects of free radicals are eliminated [94]. One of the most important diseases caused by these free radicals is diabetes mellitus. Diabetes mellitus is an endocrine and metabolic disease that occurs as a result of insulin hormone deficiency and progresses with disorders in carbohydrate, lipid, and protein metabolism [95–97]. Therefore, it is important to have antioxidant and antidiabetic substances. In this study, it was aimed at determining the in silico biological activity (antioxidant and antidiabetic) of the title compound.

Using molecular docking analyses, receptor and ligand binding sites in biological systems were identified and examined, thus understanding how the silver complex inhibits enzymes. The study of the silver complex's interaction with the proteins was conducted using AutoDock. During the investigation, ten conformations were discovered, with the best conformation signified by the lowest binding energy. The 2D interaction diagrams between the compounds and the proteins are effectively illustrated in Fig. 15. These diagrams show the importance of binding energy interactions, hydrophobic interactions, and hydrogen bonding [98,99]. The results of molecular docking studies between the synthesized compound and the crystal structures of the following proteins are shown: saccharomyces cerevisiae isomaltase α-glucosidase (Pdb: 3aj7), human pancreatic α-amylase (Pdb: 5e0f), and antioxidant cytochrome c peroxidase (CCP) (Pdb: 2×08). In accordance with biological studies, we used acarbose, a standard antidiabetic drug, as the standard for antidiabetic activity, and ascorbic acid as the standard for antioxidant activity. The docking of acarbose with α-glucosidase and α-amylase enzymes was done to confirm the docking studies that had

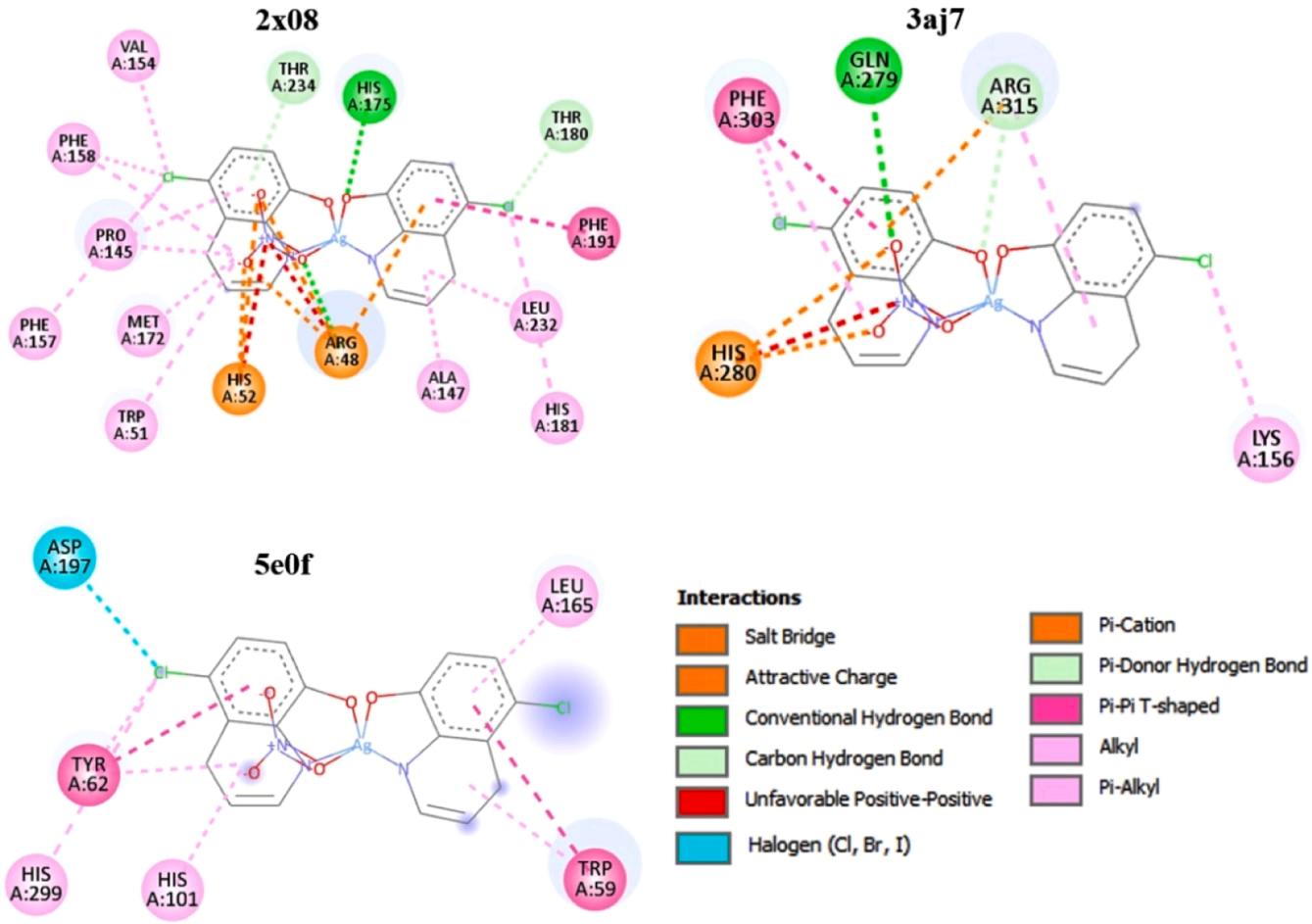

Fig. 15. 2D diagram of the receptor-compound interactions between CCP (2×08), α-Glucosidase (3aj7), α-Amylase (5e0f).

been done in previous studies [100–105]. The binding energy values that are determined through molecular docking are determined by the bond types and lengths that the ligand and proteins form [106]. The binding energy between the title compound and the α-amylase and α-glucosidase enzymes are 8.3 and 9.5 kcal/mol, respectively, while the binding energy between the antioxidant enzyme is 10.5 kcal/mol. The results of the docking study also support these data from the experimental studies. The binding of α-amylase and α-glucosidase proteins to the title compound shows better binding energy than the standard, indicating that the synthesized complex is a suitable lead compound for antidiabetic drug design. Also, ligand-peroxidase proteins have the highest docking activity than standard. When looking at the binding energy and inhibition constant (Ki) values, the α-glucosidase enzyme appears to be a more powerful potential inhibitor than α-amylase due to its lower Ki and favorable binding energy. In the in vitro study, it was determined that the complex inhibited the α-glycosidase enzyme more than it inhibited the α-amylase enzyme.

It was found that the Ag(I) complex interacts with the α-glucosidase and α-amylase enzymes in the same active pocket site as the acarbose drug. In the case of acarbose, hydrogen bonds (Gln63) and some amino acids (Trp59, Tyr62, and Leu165) formed hydrophobic contacts with active site amino acid residues of α-amylase. Looking at the detailed 2D interactions (see Fig. 15). of the docked compound within the active site of α-glucosidase, Arg279 interacts with the oxygen of the complex to provide a conventional hydrogen bond with a distance of 2.89 Å. The π-cation bond was formed between the nitrogen of Arg315 and the oxygen of the nitrate group. On the other hand, when the Ag(I) complex was docked at the binding site of the antioxidant agent, it was done via conventional hydrogen bonding with His175 (1.62 Å), carbon hydrogen bonding with Thr234 (2.25 Å), and hydrophobic interaction through Tpr51, Pro145, Phe158, Thr180, Tyr187, Leu232, and Thr234 (see Table 9). These interactions suggested favorable nonpolar contacts between the hydrophobic residues of the protein and the ligand molecule, contributing to the stability of the ligand-protein complex. The docking result indicated that the protein's active site had strong interactions with the compound, including hydrogen bonding and hydrophobic interactions [14]. These results confirm that the in experimental biological activity of the Ag(I) complex is in good agreement with the docking results and that the compound has potent in vitro antioxidant properties as well as inhibitors of α-amylase/α-glucosidase.

4. Conclusion

In this study, the new Ag(I) complex synthesized was characterized by modern spectroscopic techniques and tested to determine its ability to inhibit α-amylase, α-glucosidase, and antioxidant activity. The excellent consistency of the results obtained from DFT calculations and experimental and infrared spectra, as well as UV-Vis absorption studies, is remarkable in terms of completing the study. Fukui and MEP say that nucleophiles and electrophiles can attack the negatively charged nitrogen atom as well as the positively charged hydrogen (hydrochloride group) and oxygen atoms. The FMO of the compounds was assessed using DFT, which demonstrated their bioactivity, stability, and charge transfer. The NBO assessment revealed important donor–acceptor interactions, like LP(O) → LP*(Ag), which has the highest stabilization energy of 231.86 kcal/mol, as shown by the QTAIM and RDG analyses, demonstrating favorable findings. This topology analysis suggests that the title compound is chemically active and hence it may posses NLO applications. In vitro studies found that the complex has a stronger antioxidant effect than the standard acarbose drug and inhibits the $DPPH^{\bullet}$ radical (97.13 μg/mL) more than the $ABTS^{\bullet}+$ (109.04 μg/mL) radical, indicating potent radical scavenger activity. We conclude that the compounds mentioned have the potential to be used as therapeutic agents in the treatment of metabolic diseases, oxidative stress-related diseases, and diabetes mellitus. Molecular docking studies show that the inhibitors bind to the active sites of the enzymes and confirm the in vitro results. Consequently, it is advised that the compounds be subjected to more comprehensive experimental studies of their effects on a variety of diseases, and that this compound be further investigated in the context of candidate drug discovery.

Corresponding author declaration

The corresponding author of this manuscript, certifies that the contributors' and conflicts of interest statements included in this paper are correct and have been approved by all co-authors. I further confirm that the manuscript has been read and approved by all named authors and that there are no other persons who satisfied the criteria for authorship but are not listed. We further confirm that the order of authors listed in the manuscript has been approved by all of us.

List of Abbrevations

8-HQ = 8-hydroxyquinoline
5Cl8HQ = 5-chloroquinolin-8-ol
DFT = Density Functional Theory
B3LYP = Becke, 3-parameter, Lee-Yang-Parr
SDD = Stuttgart Dresden triple zeta ECPs Effective-Core Potential
$ABTS^{\bullet+}$ = [2,2′-Azino-bis(3-ethylbenzthiazoline-6-sulfonic acid)] cationic radical
$DPPH^{\bullet}$ = 2,2-diphenyl-1-picrylhydrazyl
IC_{50} = Inhibitor concentration

CRediT authorship contribution statement

Ceyhun Kucuk: Writing – original draft, Visualization, Validation,

Table 9
Docking parameters of the interaction title compound and acarbose with receptors.

Receptor	Compounds	Hydrogen Bonds	Hydrophobic interactions	Binding Energy (kcal/mol)	Inhibition constant K_i (μM)
Antioxidant CCP (2×08)	[Ag $(C_9H_4ClNO)_2NO_3$]	His 175, Thr 234	Tpr 51, Pro 45,Tyr 153, Phe158,Thr 180, Tyr187, Leu 232, Thr 234	-10.5	19.22
	Ascorbic Acid	Ala147, Arg48	Asc1253, Ser 81, Asp146,Ser185,Hem1254, His 52, Pro145, Tyr 187	-9.1	
α-Amylase (5e0f)	[Ag $(C_9H_4ClNO)_2NO_3$]	Gln 63	Trp 58, Tyr 62, Leu 165	-8.3	771.62
α-Glucosidase (3aj7)	Acarbose	Gln 63, Trp 59, Thr163, His 305, Tyr151, Asp197, Asp 300	Trp 58, Arg 195, His 299, His 101, Tyr 62, Leu165, Gly 306, Ala 307	-6.7	
	[Ag $(C_9H_4ClNO)_2NO_3$]	Gln 279, His 280, Arg 315	Tyr 158, Phe 303	-9.5	128.74
	Acarbose	Lys 155, Phe 157, His 245, His 280, Pro 309, Arg 315, Tyr 313, Asp 349, Asp 408	Phe 158, Gly 159, Asn 412, Ala 278, Phe 310, Phe 300, Val 303, Gln 350, Leu 437, Arg 439	-7.4	

*Standard drug: Acarbose [103], Ascorbic [106]

Supervision, Software, Resources, Methodology, Investigation, Conceptualization. **Sibel Celik:** Writing – original draft, Supervision, Software, Methodology, Investigation, Data curation, Conceptualization. **Senay Yurdakul:** Writing – original draft, Supervision, Methodology, Investigation, Data curation, Conceptualization. **Ebru Coteli:** Writing – original draft, Supervision, Methodology, Investigation, Conceptualization.

Declaration of competing interest

The authors declare that they have no known competing financial interests or personal relationships that could have appeared to influence the work reported in this paper.

Supplementary materials

Supplementary material associated with this article can be found, in the online version, at doi:10.1016/j.molstruc.2024.141285.

Data availability

No data was used for the research described in the article.

References

[1] M. Rbaa, S. Jabli, Y. Lakhrissi, M. Ouhssine, F. Almalki, T.B. Hadda, S. M. Moumene, A. Zarrouk, B. Lakhrissi, Synthesis, antibacterial properties and bioinformatics computational analyses of novel 8-hydroxyquinoline derivatives, Heliyon 5 (2019) e02689, https://doi.org/10.1016/j.heliyon.2019.e02689.

[2] S.R. Kale, M.R. Nanaware, R.S Bhondwe, Synthesis, UV-visible and ADME study of transition metal complexes of 8-Hydroxyquinoline, AJRC 3 (2) (2022) 06–10.

[3] M. Rbaa, S. Haida, B. Tuzun, A. Hichar, A. El Hassane, A. Kribii, Y. Lakhrissi, T. B. Hadda, A. Zarrouk, B. Lakhrissi, E. Berdimurodov, Synthesis, characterization and bioactivity of novel 8-hydroxyquinoline derivatives: experimental, molecular docking, DFT and POM analyses, J. Mol. Struct. 1258 (2022) 132688, https://doi.org/10.1016/j.molstruc.2022.132688.

[4] T. Damena, M.B. Alem, D. Zeleke, T.B. Demissie, T. Desalegn, Synthesis and computational studies of novel cobalt(II) and oxovanadium(IV) complexes of quinoline carbaldehyde derivative ligand for antibacterial and antioxidant applications, J. Mol. Struct. 1280 (2023) 134994, https://doi.org/10.1016/j.molstruc.2023.134994.

[5] Y. Song, H. Xu, W. Chen, P. Zhan, X. Liu, 8-Hydroxyquinoline: a privileged structure with a broad-ranging pharmacological potential, Med. Chem. Commun. 6 (2015) 61–74, https://doi.org/10.1039/C4MD00284A.

[6] S.S. Sharma, P. Yadav, S. Kumari, M. Ranka, Synthesis and structural elucidation of 1,2naphthoquinone derivatives, Schiff base complexes and ternary complexes with 8hydroxyquinoline: comparative studies of their antimicrobial, antiinflammatory and antidiabetic activities, Transit. Met. Chem. 48 (2023) 389–400, https://doi.org/10.1007/s11243-023-00551-w.

[7] A. Ali, S. Banerjee, S. Kamaal, M. Usman, N. Das, M. Afzal, A. Alarifi, N. Sepay, M. Ahmad, Ligand substituent effect on the cytotoxicity activity of two new copper(II) complexes bearing 8 hydroxyquinoline derivatives: validated by MTT assay and apoptosis in MCF-7 cancer cell line (human breast cancer), RSC Adv. 11 (2021) 14362, https://doi.org/10.1039/d1ra00172h.

[8] H.W. Lee, H.S. Lee, 2-Hydroxyquinoline and its structural analogs show antidiabetic effects against α-amylase and α-glucosidase, J. Appl. Biol. Chem. 58 (1) (2015) 1–3, https://doi.org/10.3839/JABC.2015.001.

[9] B.N. Socha, Sachin B. Pandya, Urmila H. Patel, R.H. Patel, Structural investigation, quantum chemical calculation, energy framework analysis and MIC studies of silver and cobalt complexes of 4-amino-N-(4, 6-dimethyl-2 pyrimidinyl) benzenesulfonamide in presence of secondary ligand, Inorg. Chem. Commun. 154 (2023) 110936, https://doi.org/10.1016/j.inoche.2023.110936.

[10] N. Shayegan, S. Haghipour, N. Tanideh, A. Moazzam, S. Mojtabavi, M. A. Faramarzi, C. Irajie, S. Parizad, S. Ansari, B. Larijani, S. Hosseini, A. Iraji, M. Mahdavi, Synthesis, in vitro αglucosidase inhibitory activities, and molecular dynamic simulations of novel 4hydroxyquinolinonehydrazones as potential antidiabetic agents, Sci. Rep. 13 (2023) 6304, https://doi.org/10.1038/s41598-023-32889-7.

[11] Ö. Özge, D. Avcı, F. Sönmez, Ö. Tamer, N. Dege, A. Basoglu, Y. Atalay, B.Z. Kurt, Synthesis, DFT calculations, α-glucosidase inhibitor activity, and docking studies on Schiff base metal complexes containing isothiocyanate, Appl. Organomet. Chem. 37 (5) (2023) e7084, https://doi.org/10.1002/aoc.7084.

[12] A.J. Kadhium, B.S. Abdulmahdi, F.J. Ali, Preparation, determination and study toxicity effects of new mixed ligands complexes derivative from 8- hydroxy quinoline with Pd(II), Egypt. J. Chem. Vol. 64 (9) (2021) 5283–5288, https://doi.org/10.21608/ejchem.2021.73861.3652.

[13] F. Prati, C. Bergamini, R. Fato, O. Soukup, J. Korabecny, V. Andrisano, M. Bartolini, M. Bolognesi, Novel 8-hydroxyquinoline derivatives as multitarget compounds for the treatment of Alzheimer's disease, Chem. Med. Chem. 11 (2016) 1284–1295, https://doi.org/10.1002/cmdc.201600014.

[14] H.M.A. El-Lateef, M.M. Khalaf, F.E.T. Heakal, A. Ahsa, A. Abdou, Fe(III), Ni(II), and Cu(II)-moxifloxacin-tri-substituted imidazole mixed ligand complexes: synthesis, structural, DFT, biological, and protein-binding analysis, Inorg. Chem. Commun. 158 (2023) 111486, https://doi.org/10.1016/j.inoche.2023.111486.

[15] B. Honarparvar, T. Govender, G.E.M. Maguire, M.E.S. Soliman, H,G. Kruger, Integrated approach to structure-based enzymatic drug design: molecular modeling, spectroscopy, and experimental bioactivity, Chem. Rev. 114 (1) (2014) 493–537, https://doi.org/10.1021/cr300314q.

[16] M.J. Frisch, G.W. Trucks, H.B. Schlegel, G.E. Scuseria, M.A. Robb, J.R. Cheeseman, G. Scalmani, V. Barone, B. Mennucci, G.A. Petersson, H. Nakatsuji, M. Caricato, X. Li, H.P. Hratchian, A.F. Izmaylov, J. Bloino, G. Zheng, J.L. Sonnenberg, M. Hada, M. Ehara, K. Toyota, R. Fukuda, J. Hasegawa, M. Ishida, T. Nakajima, Y. Honda, O. Kitao, H. Nakai, T. Vreven, J.A. Montgomery, Jr., J.E. Peralta, F. Ogliaro, M. Bearpark, J.J. Heyd, E. Brothers, K.N. Kudin, V.N. Staroverov, R. Kobayashi, J. Normand, K. Raghavachari, A. Rendell, J.C. Burant, S.S. Iyengar, J. Tomasi, M. Cossi, N. Rega, J.M. Millam, M. Klene, J.E. Knox, J.B. Cross, V. Bakken, C. Adamo, J. Jaramillo, R. Gomperts, R.E. Stratmann, O. Yazyev, A.J. Austin, R. Cammi, C. Pomelli, J.W. Ochterski, R.L. Martin, K. Morokuma, V.G. Zakrzewski, G.A. Voth, P. Salvador, J.J. Dannenberg, S. Dapprich, A.D. Daniels, O. Farkas, J.B. Foresman, J. V. Ortiz, J. Cioslowski, D.J. Fox, Gaussian 09, Gaussian, Inc., Wallingford CT, (2009).

[17] R. Dennington, T. Keith, J. Millam, GaussView, Version 5, Semichem Inc., Shawnee Mission, KS, USA. (2009).

[18] A.D. Becke, Density-functional thermochemistry III. The role of exact exchanege, J. Chem. Phys. 98 (1993) 5648–5652, https://doi.org/10.1063/1.464913.

[19] C. Lee, W. Yang, R.G. Parr, Development of the çolle-salvetti¨correlation-energy formula into a functional of the electron density, Phys. Rev. B37 (1988) 785–789, https://doi.org/10.1103/PhysRevB.37.785.

[20] R.J. Davidson, E.W. Ainscough, A.M. Brodie, G.B. Jameson, M.R. Waterland, Chemical and physical behaviour of heteroleptic 2,6-bis(1*H*-benzimidazol-2-yl) pyridine and 2,2′:6′,2″-terpyridine substituted tricyclophosphazene ruthenium(II) complexes, Polyhedron 103 (B) (2016) 217–226, https://doi.org/10.1016/j.poly.2015.02.018.

[21] J.S. Al-Otaibi, Y.S. Mary, Y.S. Mary, M.C. Gamberini, Revealing the adsorption of sulfanilamide on pristine Ag3, Au3, Cu3 and AgAuCu clusters: sensing mechanism, SERS activity and docking studies by DFT, Comput. Theor. Chem. 1237 (2024) 114662, https://doi.org/10.1016/j.comptc.2024.114662.

[22] L.G. Ramírez-Palma, A. Espinoza-Guillén, F. Nieto-Camacho, A.E. López-Guerra, V. Gómez-Vidales, F. Cortés-Guzmán, L. Ruiz-Azuara, Intermediate detection in the casiopeina–cysteine interaction ending in the disulfide bond formation and copper reduction, Molecules 26 (19) (2021) 5729, https://doi.org/10.3390/molecules26195729.

[23] H. Yousfi, N.E.H. Bensiradj, M. Khedidji, A. Saal, O. Ouamerali, Theoretical investigation of the structure and spectroscopy of uranium oxide species, Theor. Chem. Acc. 14 (5) (2023), https://doi.org/10.1007/s00214-022-02947-w.

[24] H.B. Howsaui, A.S. Basaleh, M.H. Abdellattif, W.M.I. Hassan, M.A. Hussien, Synthesis, structural investigations, molecular docking, and anticancer activity of some novel Schiff bases and their uranyl complexes, Biomolecules 11 (8) (2021) 1138, https://doi.org/10.3390/biom11081138.

[25] S. Celik, DFT investigations and molecular docking as potent inhibitors of SARS-CoV-2 main protease of 4-phenylpyrimidine, J. Mol. Struct. 1277 (2023) 134895, https://doi.org/10.1016/j.molstruc.2022.134895.

[26] B. Silvi, A. Savin, Classification of chemical bonds based on topological analysis of electron localization functions, Nature 371 (6499) (1994) 683–686, https://doi.org/10.1038/371683a0.

[27] A.R. Kumar, L. Ilavarasan, G.P.S. Mol, S. Selvaraj, M. Azam, P. Jayaprakash, M. Kesavan, M. Alam, J. Dhanalakshmi, S.I. Al-Resayes, A. Ravi, Spectroscopic (FT-IR, FT-Raman, UV–Vis and NMR) and computational (DFT, MESP, NBO, NCI, LOL, ELF, RDG and QTAIM) profiling of 5-chloro-2-hydroxy-3-methoxybenzaldehyde: a promising antitumor agent, J. Mol. Struct. 1298 (1) (2024) 136974, https://doi.org/10.1016/j.molstruc.2023.136974.

[28] G.M. Morris, D.S. Goodwill, R.S. Halliday, R. Huey, W. Hart, R.K. Belew, A. J. Olson, Automated docking using a Lamarckian genetic algorithm and an empirical binding free energy function, J. Comput. Chem. 19 (1998) 1639, https://doi.org/10.1002/(SICI)1096-987X(19981115)19, 14<1639::AID-JCC10>3.0.CO;2-B.

[29] Dassault Systemes BIOVIA, Discovery Studio Modeling Environment, Release 2017, Dassault Systemes, San Diego, 2016.

[30] O.P. Sharma, T.K. Bhat, DPPH antioxidant assay revisited, Food Chem. 113 (4) (2009) 1202–1205, https://doi.org/10.1016/j.foodchem.2008.08.008.

[31] C.A. Rice-Evans, Screening of Phenolics And Flavonoids For Antioxidant Activity, Elsevier: Academic Press, 1999, pp. 239–253, https://doi.org/10.1016/B978-012543590-1/50017-2.

[32] E. Apostolidis, Y.I. Kwon, K. Shetty, Inhibitory potential of herb, fruit, and fungal-enriched cheese against key enzymes linked to type 2 diabetes and hypertension, Innov. Food Sci. Emerg. Technol. 8 (2007) 46–54, https://doi.org/10.1016/j.ifset.2006.06.001.

[33] D.M. Casirola, R.P. Ferraris, α-Glucosidase inhibitors prevent diet-induced increases in intestinal sugar transport in diabetic mice, Metabolism 55 (2006) 832–841, https://doi.org/10.1016/j.metabol.2006.02.011.

[34] Y.I. Kwon, E. Apostolidis, K. Shetty, Inhibitory potential of wine and tea aganist a-amylase and aglucosidase for management of hyperglycemia linked to type 2 diabetes, J. Food Biochem. 32 (2008) 15–31, https://doi.org/10.1111/j.1745-4514.2007.00165.x.

[35] J.E. Fleming, H. Lynt, Crystal and molecular structure of the pyridine solvate of bis(8-hydroxyquinoline)silver(I), Can. J. Chem. 46 (4) (1968), https://doi.org/10.1139/v68-079.
[36] H. Wu, X.W. Dong, J.F. Ma, Aqua(8-hydroxyquinoline-5-sulfonato-*j*2N,O8)-silver (I) monohydrate, Acta Crystallogr. Sect. E E62 (2006) m385–m387, https://doi.org/10.1107/S1600536806002947.
[37] Z. Ma, B. Moulton, 5-Chloro-8-hydroxyquinoline, CCDC 687619: Experimental Crystal Structure Determination, 2010.
[38] T. Sundius, S.A. Brandan, Structural, harmonic force field and vibrational studies of cholinesterase inhibitor tacrine used for treatment of Alzheimer's disease, Heliyon 9 (2023) e717280, https://doi.org/10.1016/j.heliyon.2023.e17280.
[39] A.B. Rached, W. Maalej, P. Guionneau, N. Daro, T. Mhiri, H. Feki, Z. Elaoud, Synthesis, crystal structure, and vibrational and dft simulation studies of benzylammonium dihydrogen phosphate, J. Phys. Chem. Solids 123 (2018) 150–156, https://doi.org/10.1016/j.jpcs.2018.07.017.
[40] S.S.S Abuthahir, A.J.A. Nasser, S. Rajendran, G. Brindha, Synthesis, spectral studies and antibacterial activities of 8-hydroxyquinoline derivative and its metal complexes, Chem. Sci. Trans. 3 (1) (2014) 303–313, https://doi.org/10.7598/cst2014.641.
[41] M.L. Ramos, L.L.G. Justino, S.M. Fonseca, H.D. Burrows, NMR, DFT and luminescence studies of the complexation of V(V) oxoions in solution with 8-hydroxyquinoline-5-sulfonate, New J. Chem. 39 (2015) 1488, https://doi.org/10.1039/c4nj01873g.
[42] S. Selveraj, P. Rajkumar, M. Kesavan, K. Mohanraj, S. Gunasekaran, S. Kumaresan, A combined experimental and theoretical study on 4-hydroxy carbazole by FT-IR, FT-Raman, NMR, UV–visible and quantum chemical investigations, CDC 17-18 (2018) 302–311, https://doi.org/10.1016/j.cdc.2018.10.003.
[43] S.M. Soliman, Molecular structure and vibrational spectra of free and coordinated 3-bromoquinoline: unexpected intramolecular C-H ···interactions, J. Mol. Struct. 1017 (2012) 135–142, https://doi.org/10.1016/j.molstruc.2012.03.016.
[44] C. Kucuk, S. Celik, S. Yurdakul, E. Cotelı, B. Erdem, Synthesis, characterization, thermal, DFT study, antioxidant and antimicrobial in vitro investigations of indazole and its Ag(I) complex, Polyhedron 241 (2023) 116469, https://doi.org/10.1016/j.poly.2023.116469.
[45] V. Sathyanarayanmoorthi, R. Karunathan, V. Kannappan, Molecular modeling and spectroscopic studies of benzothiazole, J. Chem. (2013) 258519, https://doi.org/10.1155/2013/258519.
[46] A.R. Kumar, N. Kanagathara, S. Selvaraj, Spectroscopic, structural and molecular docking studies on N,N-dimethyl-2-[6-methyl-2-(4-methylphenyl) imidazo[1,2-a] pyridin-3-yl] acetamide, Phys. Chem. Res. 12 (1) (2024) 95–107, https://doi.org/10.22036/pcr.2023.387911.2306.
[47] S. Selvaraj, P. Rajkumar, M. Kesavan, S. Gunasekaran, S. Kumaresan, R. Rajasekar, T.S.R. Devi, Spectroscopic and quantum chemical investigations on structural isomers of dihydroxybenzene, J. Mol. Struct. 1196 (2019) 291–305, https://doi.org/10.1016/j.molstruc.2019.06.075.
[48] S. Celik, S. Yurdakul, B. Erdem, New silver(I) complex as antibiotic candidate: synthesis, spectral characterization, DFT, QTAIM and antibacterial investigations and docking properties, J. Mol. Struct. 1261 (2022) 132902, https://doi.org/10.1016/j.molstruc.2022.132902.
[49] C. Kucuk, S. Celik, S. Yurdakul, B. Erdem, Experimental and DFT studies of 2-methyl-quinoxaline and its silver (I) complex: non-covalent interaction analysis, antimicrobial activity and molecular docking study, Inorg. Chem. Commun. 145 (2022) 109935, https://doi.org/10.1016/j.inoche.2022.109935.
[50] S. Celik, S. Yurdakul, B. Erdem, Synthesis, spectroscopic characterization (FT-IR, PL), DFT calculations and antibacterial activity of silver(I) nitrate complex with nicotinaldehyde, Inorg. Chem. Commun. 131 (2021) 108760, https://doi.org/10.1016/j.inoche.2021.108760.
[51] V. Arjunan, L. Devi, R. Subbalakshmi, T. Rani, S. Mohan, Synthesis, vibrational, NMR, quantum chemical and structure-activity relation studies of 2-hydroxy-4-methoxyacetophenone, Spectrochim. Acta A Mol. Biomol. Spectrosc. 130 (2014) 164–177, https://doi.org/10.1016/j.saa.2014.03.121.
[52] P. Rajkumar, S. Selvaraj, R. Suganya, M. Kesavan, G. Serdaroğlu, S. Gunasekaran, S. Kumaresan, Experimental and theoretical investigations on electronic structure of 5-(hydroxymethyl)-2-furaldehyde: an antisickling agent identified from terminalia bellirica, CDC 29 (2020) 100498, https://doi.org/10.1016/j.cdc.2020.100498.
[53] V.K. Choudhary, A.K. Bhatt, D. Dash, N. Sharma, DFT calculations on molecular structures, HOMO–LUMO study, reactivity descriptors and spectral analyses of newly synthesized diorganotin(IV) 2-chloridophenylacetohydroxamate complexes, J. Comput. Chem. 40 (2019) 2354–2363, https://doi.org/10.1002/jcc.26012.
[54] S.E. Ashoor, R.A. Abokhater, L. Belkhiri, S.A. Gadir, Spectroscopy and DFT studies on Cr(III) complexes with saccharides, 8-hydroxyquinoline and their biological activity, J. Mol. Struct. 1281 (2023) 135134, https://doi.org/10.1016/j.molstruc.2023.135134.
[55] M.J. Alam, A.U. Khan, M. Alam, S. Ahmad, Spectroscopic (FTIR, FT-Raman, 1H NMR and UV–Vis) and DFT/TD-DFT studies on cholesteno [4,6-b,c]-2′,5′-dihydro-1′,5′-benzothiazepine, J. Mol. Struct. 1178 (2019) 570–582, https://doi.org/10.1016/j.molstruc.2018.10.063.
[56] P. Shafieyoon, İ. Mehdipur, Y.S. Mary, Synthesis, characterization and biological investigation of glycine-based sulfonamide derivative and its complex: vibration assignment, HOMO – LUMO analysis, MEP and molecular docking, J Mol. Struct. 1181 (2019) 244–252, https://doi.org/10.1016/j.molstruc.2018.12.067.
[57] O.M. Adly, H.F. El-Şafiy, New metal complexes derived from *S*-benzyldithiocarbazate (SBDTC) and chromone-3-carboxaldehyde: synthesis, characterization, antimicrobial, antitumor activity and DFT calculations, J. Coord. Chem. 72 (2) (2019) 218–238, https://doi.org/10.1080/00958972.2018.1564912.
[58] R.T. Ulahannan, C.Y. Panicker, H.T. Varghese, R. Musiol, J. Jampilek, C. V. Alsenoy, J.A. War, T.K. Manojkumar, Vibrational spectroscopic studies and molecular docking study of 2-[(*E*)-2-phenylethenyl]quinoline-5-carboxylic acid, Spectrochim. Acta A Mol. Biomol. Spect. 150 (2015) 19–199, https://doi.org/10.1016/j.saa.2015.04.104.
[59] B. Sureshkumar, Y. Sheena Mary, S. Suma, S. Armaković, S.J. Armaković, C. V. Alsenay, B. Narayana, B.P. Sasidharan, Spectroscopic characterization of 8-hydroxy-5-nitroquinoline and 5-chloro-8-hydroxy quinoline and investigation of its reactive properties by DFT calculations and molecular dynamics simulations, J. Mol. Struct. 1164 (2018) 525–538, https://doi.org/10.1016/j.molstruc.2018.03.088.
[60] A. Suhta, S. Saral, U. Çoruh, S. Karakuş, E.M.V. Lopez, Synthesis, single crystal X-ray, hirshfeld surface analysis and DFT calculation based NBO, HOMO–LUMO, MEP, ECT and molecular docking analysis of N′-[(2,6-dichlorophenyl) methylidene]-2-{[3-(trifluoromethyl)phenyl]amino}benzohydrazide, J. Struct. Chem. 65 (2024), https://doi.org/10.1134/S0022476624010189, 196-195.
[61] H. Kargar, M.F. Mehrjardi, R.B. Ardakani, K.S. Munawar, M. Ashfaq, M.N. Tahir, Diverse coordination of isoniazid hydrazone Schiff base ligand towards iron(III): synthesis, characterization, SC-XRD, HSA, QTAIM, MEP, NCI, NBO and DFT study, J. Mol. Struct. 1250 (2022) 131691, https://doi.org/10.1016/j.molstruc.2021.131691.
[62] K. Thirunavukkarasu, P. Rajkumar, S. Selvaraj, S. Gunasekaran, S. Kumaresan, Electronic structure, vibrational (FT-IR and FT-Raman), UV–Vis and NMR analysis of 5-(4-(2-(5-ethylpyridin-2-yl) ethoxy) benzyl) thiazolidine-2,4-dione by quantum chemical method, CDC 17-18 (2018) 263–275, https://doi.org/10.1016/j.cdc.2018.09.006.
[63] M.A. Mumit, T.K. Pal, M.A. Alam, A.A.M. Islama, S. Paul, M.C. Sheikh, DFT studies on vibrational and electronic spectra, HOMO–LUMO, MEP, HOMA, NBO and molecular docking analysis of benzyl-3N-(2,4,5-trimethoxyphenylmethylene) hydrazinecarbodithioate, J. Mol. Struct. 1220 (2020) 128715, https://doi.org/10.1016/j.molstruc.2020.128715.
[64] R.R. Saravanan, S. Seshadri, S Gunasekaran, R.M. Mendoza, S.G. Granda, Conformational analysis, X-ray crystallographic, FT-IR, FT-Raman, DFT, MEP and molecular docking studies on 1-(1-(3-methoxyphenyl) ethylidene) thiosemicarbazide, Spectrochim. Acta A Mol. Biomol. Spect. 139 (2015) 321–328, https://doi.org/10.1016/j.saa.2014.12.026.
[65] S. Yurdakul, E. Temel, O. Buyukgungor, Crystal structure, spectroscopic characterization, thermal properties and theoretical investigations on Ag(methyl 4-pyridyl ketone)2NO3], J. Mol. Struct. 1191 (2019) 301–313, https://doi.org/10.1016/j.molstruc.2019.04.071.
[66] Z. Demircioğlu, Ç.A. Kaştaş, O. Büyükgüngör, The spectroscopic (FT-IR, UV-vis), Fukui function, NLO, NBO, NPA and tautomerism effect analysis of (E)-2-[(2-hydroxy-6-methoxybenzylidene)amino]benzonitrile, Spectrochim. Acta A Mol. Biomol. Spect. 139 (2015) 539–548, https://doi.org/10.1016/j.saa.2014.11.078.
[67] P.W. Ayers, R.G. Parr, Variational principles for describing chemical reactions: the fukui function and chemical hardness revisited, J. Am. Chem. Soc. 122 (9) (2000) 2010–2018, https://doi.org/10.1021/ja9924039.
[68] A. Sethi, R.P. Singh, D. Shukla, P. Singh, Synthesis of novel pregnane-diosgenin prodrugs via Ring A and Ring A connection: a combined experimental and theoretical studies, J. Mol. Struct. 1125 (2016) 616–623, https://doi.org/10.1016/j.molstruc.2016.07.020.
[69] B.Q. Sheeba, M.S.M. Mary, M. Amalanathan, C.B. Job, Structural and vibrational spectral investigation on the identification of non-linear optical properties and wave function analyses (electrostatic potential, electron localisation function, localised orbital locator) of 3-ethoxy salicilaldehyde, Mol. Simul. 47 (15) (2021) 1217–1233, https://doi.org/10.1080/08927022.2021.1962862.
[70] A.D. Steffy, D.A. Dhas, I.H. Joe, S. Balachandran, Theoretical investigations on structural, spectral, NBO, NLO and topology exploration (AIM, ELF, LOL, RDG) of piperazine-2,5-dione oxalic acid monohydrate, J. Mol. Struct. 1295 (2) (2024) 136653, https://doi.org/10.1016/j.molstruc.2023.136653.
[71] S. Sundaram, V.N. Vijayakumar, V. Balasubramanian, Electronic and structure conformational analysis (HOMO-LUMO, MEP, NBO, ELF, LOL, AIM) of hydrogen bond binary liquid crystal mixture: DFT/TD-DFT approach, Comput. Theor. Chem. 1217 (2022) 113920, https://doi.org/10.1016/j.comptc.2022.113920.
[72] K. Arulaabaranam, S. Muthu, G. Mani, A.S. Ben Geoffrey, Speculative assessment, molecular composition, PDOS, topology exploration (ELF, LOL, RDG), ligand-protein interactions on 5-bromo-3-nitropyridine-2-carbonitrile, Heliyon 7 (5) (2021) e07061, https://doi.org/10.1016/j.heliyon.2021.e07061.
[73] K. Arulaabaranam, G. Mani, S. Muthu, Computational assessment on wave function (ELF, LOL) analysis, molecular confirmation and molecular docking explores on 2-(5-Amino-2- Methylanilino)-4-(3-pyridyl) pyrimidine, Chem. Data Collect. 29 (2020) 100525, https://doi.org/10.1016/j.cdc.2020.100525.
[74] A.R. Guerroudj, E.U. Mughal, N. Naeem, A. Sadiq, J.H. Al-Fahemi, B.H. Asghar, N. Boukabcha, A. Chouaih, S.A. Ahmed, Exploring pyrimidine-based azo dyes: vibrational spectroscopic assignments, TD-DFT investigation, chemical reactivity, HOMO-LUMO, ELF, LOL and NCI-RDG analysis, Spectrochim. Acta A Mol Biomol. Spect. 313 (2024) 124093, https://doi.org/10.1016/j.saa.2024.124093.
[75] S. Sindhuja, M. Karnan, R. Gayathri, M. Kavimani, Non-covalent interaction, topology, molecular properties, spectral and quantum chemical analysis of 2,5-dinitrophenol, J. Indian Chem. Soc. 101 (10) (2024) 101276, https://doi.org/10.1016/j.jics.2024.101276.
[76] J. Sampathkumar, R. Rajamanickam, Synthesis, crystal structure, Hirshfeld surface, QTAIM, NCI-RDG, DFT and molecular docking studies of 4-(aryl)-1,4-

dihydro-N,1-dimethyl-6-(methylthio)-3,5-dinitropyridin-2-amines, J. Mol. Struct 1299 (2024) 137063, https://doi.org/10.1016/j.molstruc.2023.137063.
[77] V.S.J. Reeda, S. Sakthivel, P. Divya, S. Javed, V.B. Jothy, Conformational stability, quantum computational (DFT), vibrational, electronic and non-covalent interactions (QTAIM, RDG and IGM) of antibacterial compound N-(1-naphthyl) ethylenediamine dihydrochloride, J. Mol. Struct. 1298 (2024) 137043, https://doi.org/10.1016/j.molstruc.2023.137043.
[78] S.K. Panja, S. Kumar, B. Haddad, A.R. Patel, D. Villemin, H.M. Amine, S. Bera, M. Debdab, Role of multiple intermolecular H-bonding interactions in molecular cluster of hydroxyl-functionalized imidazolium ionic liquid: an experimental, topological, and molecular dynamics study, Physchem 4 (4) (2024), https://doi.org/10.3390/physchem4040026, 396-388.
[79] P. Divya, V.S.J. Reeda, R. Suja, V.B. Jothy, Structural activity, spectroscopic, Fukui, NCI, AIM, IGM combined with molecular docking and molecular dynamics simulation on 4-methylpyridinium 4-hydroxybenzoate-potent drug anti-leukemia cancer, Spectrochim. Acta A Mol. Biomol. Spect. 306 (2024) 123568, https://doi.org/10.1016/j.saa.2023.123568.
[80] R.A. Khan, M.H. Jaafar, A. Paul, A. Alsalme, Structural, spectroscopic, and chemical bonding analysis of luminescent bis(diphenylphosphino)methane derived binuclear heteroleptic silver(I) complex of norharmane with argentophilic interaction, Inorg. Chim. Acta 560 (2024) 121834, https://doi.org/10.1016/j.ica.2023.121834.
[81] R. Sukanya, D. Aruldhas, I. HubertJoe, S. Balachandran, Synthesis, spectroscopic (FTIR, FT-Raman and UV-Vis), structural investigation, chemical reactivity, AIM, NBO, NLO, Hirshfeld analysis of 4-aminobenzoic acid pyrazinoic acid, Polyc. Arom. Comp. 44 (1) (2023) 25–50, https://doi.org/10.1080/10406638.2023.2165513.
[82] S.B. Kedare, R.P. Singh, Genesis and development of DPPH method of antioxidant assay, J. Food Sci. Tech. 48 (4) (2011) 412–422, https://doi.org/10.1007/s13197-011-0251-1.
[83] M. Ozgen, R.N. Reese, A.Z. Tulio, J.C. Scheerens, A.R. Miller, Modified 2,2-azino-bis3-ethylbenzothiazoline-6-sulfonic acid (ABTS) method to measure antioxidant capacity of selected small fruits and comparison to ferric reducing antioxidant power (FRAP) and 2,2 '-diphenyl-1-picrylhydrazyl (DPPH) methods, J. Agric. Food Chem. 54 (2006) 1151–1157, https://doi.org/10.1021/JF051960D.
[84] E.N. Frankel, A.S. Meyer, The problems of using one dimensional methods to evaluate multifunctional food and biological antioxidants, J. Sci. Food. Agric. 80 (2000) 1925–1941, https://doi.org/10.1002/1097-0010(200010)80, 13<1925::AID-JSFA714>3.0.CO;2-4.
[85] R. Scherer, H.T. Godoy, Antioxidant activity index (AAI) by the 2,2-diphenyl-1-picrylhydrazyl method, Food Chem. 112 (3) (2009) 654, https://doi.org/10.1016/j.foodchem.2008.06.026.
[86] J. Deng, W. Cheng, G. Yang, A novel antioxidant activity index (AAU) for natural products using the DPPH assay, Food Chem. 125 (4) (2011) 1430, https://doi.org/10.1016/j.foodchem.2010.10.031.
[87] M. Kepeňová, M. Kello, R. Smolková, M. Goga, R. Frenák, L'. Tkáčiková, M. Litecká, J. Šubrt, I. Potočňák, Low-dimensional compounds containing bioactive ligands. Part XIX: crystal structures and biological properties of copper complexes with halogen and nitro derivatives of 8-hydroxyquinoline, Inorganics 10 (2022) 223, https://doi.org/10.3390/inorganics10120223.
[88] G. Wang, D. He, X. Li, J. Li, Z. Peng, Design, synthesis and biological evaluation of novel coumarin thiazole derivatives as α-glucosidase inhibitors, Bioorg. Chem. 65 (2016) 167–174, https://doi.org/10.1016/j.bioorg.2016.03.001.
[89] N. Kaur, V. Kumar, S.K. Nayak, P. Wadhwa, P. Kaur, S.K. Sahu, Alpha- amylase as molecular target for treatment of diabetes mellitus: a comprehensive review, Chem. Biol. Drug Des. 98 (4) (2021) 539–560, https://doi.org/10.1111/cbdd.13909.
[90] Z. Fallah, M. Tajbakhsh, M. Alikhani, B. Larijani, M.A. Faramarzi, H. Hamedifar, M. Mahdavi, A review on synthesis, mechanism of action, and structure-activity relationships of 1, 2, 3-triazole-based α-glucosidase inhibitors as promising anti-diabetic agents, J. Mol. Struct. 1255 (2022) 132469, https://doi.org/10.1016/j.molstruc.2022.132469.
[91] D. Satheesh, R. Roshini, S. Jeevitha, K. Chithra, S.V. Kumar, P. Sellam, Anti-inflammatory and anti-diabetic activity of 8-hydroxyquinolinium 3,5-dinitrobenzoate, Chem. Data Coll. 33 (2021) 100726, https://doi.org/10.1016/j.cdc.2021.100726.
[92] P. Divya, V.S.J. Reeda, V.B. Jothy, Fungicide compound 2, 3-dichloronaphthalene-1, 4-dione: non-covalent interactions (QTAIM, RDG and ELF), combined vibrational spectroscopic investigations using DFT approach with experimental analysis, electronic, molecular docking scrutiny in-vitro assay and thermodynamic property analysis, J. Mol. Liquids 400 (2024) 124544, https://doi.org/10.1016/j.molliq.2024.124544.
[93] P.M. Clarkson, H.S. Thompson, Antioxidants: what role do they play in physical activity and health, Am. J. Clin. Nutr. 72 (2000) 637–646, https://doi.org/10.1093/ajcn/72.2.637S.
[94] D. Barber, S. Harris, Oxygen free radicals and antioxidants. A review, Am. Pharma. 9 (1994) 26–35, https://doi.org/10.1016/S0160-3450(15)30310-X.
[95] A.M. Vincent, J.W. Russell, P. Low, E.L. Feldman, Oxidative stress in the pathogenesis of diabetic neuropathy, Endocr. Rev. 25 (2004) 612–628, https://doi.org/10.1210/er.2003-0019.
[96] R. Memisogullari, S. Taysi, E. Bakan, I. Capoglu, Antioxidant status and lipid peroxidation in type II diabetes mellitus, Cell Biochem. Funct. 21 (2003) 291–296, https://doi.org/10.1002/cbf.1025.
[97] A. Cherubini, C. Ruggiero, M.C. Polidori, C. Mecocci, Potential markers of oxidative stress in stroke, Free Radic. Biol. Med. 39 (2005) 841–852, https://doi.org/10.1016/j.freeradbiomed.2005.06.025.
[98] S.Selvaraj A.R.Kumar, P. Rajkumar, J. Dhanalakshmi, S.K.Nagarajan M.Kumar, P. Jayaprakash, G.P. Sheeja Mol, S. Awasthi, S.K. Pandey, Insights into structural, vibrational, and chemical shift characteristics, solvents impact (polar and nonpolar) on electronic properties and reactive sites, ADMET predictions, and ligand-protein interactions for antiviral drugs safrole and isosafrole: an in-silico approach, Chem. Phys. Impact 8 (2024) 100443, https://doi.org/10.1016/j.chphi.2023.100443.
[99] A.R. Kumar, S. Selvaraj, A.S. Vickram, G.P. Sheeja Mol, S. Awasthi, M. Thirunavukkarasu, M. Selvaraj, S. Basumatary, Exploring the potential of diosgenin as a promising antitumor agent through comprehensive spectroscopic characterization, solvent–solute interactions, topological properties, Hirshfeld surface, and molecular docking interactions with 2NZT and 2I1V proteins, Spectrochim. Acta - A Mol. Biomol. Spectrosc. 327 (2025) 125349, https://doi.org/10.1016/j.saa.2024.125349.
[100] U. Ghani, S. Ashraf, Z.U. Haq, Z.A. Kaplancikli, F. Demirci, Y. Ozkay, S. Afzal, Thiazole inhibitors of α-glucosidase: positional isomerism modulates selectivity, enzyme binding and potency of inhibition, Comput. Biol. Chem. 98 (2022) 107647, https://doi.org/10.1016/j.compbiolchem.2022.107647.
[101] M.M. Khalifa, H.M. Sakr, A. Ibrahim, A.M. Mansour, R.R. Ayyad, Design and synthesis of new benzylidene-quinazolinone hybrids as potential anti-diabetic agents: in vitro α-glucosidase inhibition, and docking studies, J. Mol. Struct. 1250 (2022) 131768, https://doi.org/10.1016/j.molstruc.2021.131768.
[102] J.H. Zhang, H.X. Xie, Y. Li, K.M. Wang, Z. Song, K.K. Zhu, L. Fang, J. Zhang, C. S. Jiang, Design, synthesis and biological evaluation of novel (E)-2-benzylidene-N- (3-cyano-4, 5, 6, 7-tetrahydrobenzo [b] thiophen-2-yl) hydrazine-1-carboxamide derivatives as α-glucosidase inhibitors, BMCL 52 (2021) 128413, https://doi.org/10.1016/j.bmcl.2021.128413.
[103] M. Taha, N.H. Ismail, S. Imran, A. Wadood, F. Rahim, S.M. Saad, K.M. Khan, A. Nasir, Synthesis, molecular docking and α-glucosidase inhibition of 5-aryl-2-(6 nitrobenzofuran-2 '-yl)-1, 3, 4-oxadiazoles, Bioorg. Chem. 66 (2016) 9241, https://doi.org/10.1016/j.bioorg.2016.04.006, 117–123.
[104] S. Zahra, S. Zaib, I. Khan, Identification of isobenzofuranone derivatives as promising antidiabetic agents: synthesis, in vitro and in vivo inhibition of α-glucosidase and α-amylase, computational docking analysis and molecular dynamics simulations, Int. J. Biol. Macromol. 259 (2) (2024) 129241, https://doi.org/10.1016/j.ijbiomac.2024.129241.
[105] F. Çelik, Y. Ünver, F. Oztuncay, U. Cakmak, Y. Kolcuoglu, K.K. Uzun, H. Ozturk, N. Yorulmaz, I. Değirmencioğlu, Synthesis and characterization of newly phthalocyanine molecules: their enzyme inhibition and antioxidant properties, in silico and in vitro, J. Organomet. Chem. 1016 (2024) 123237, https://doi.org/10.1016/j.jorganchem.2024.123237.
[106] R. Ahmad, A. Alam, M. Khan, T. Ali, A.A. Elhenawy, M. Ahmad, Antioxidant activity, molecular docking and quantum studies of NewBis-Schiff bases based on benzyl phenyl ketone moiety, ChemistrySelect 8 (15) (2023) e202302338, https://doi.org/10.1002/slct.202302338.